

Petrochemical evidence of magma mingling and mixing in the Tertiary monzogabbroic stocks around the Bafra (Samsun) area in Turkey: implications of coeval mafic and felsic magma interactions

İrfan Temizel

Received: 12 October 2012 / Accepted: 7 July 2013 / Published online: 11 August 2013
© Springer-Verlag Wien 2013

Abstract Miocene aged calc-alkaline mafic host stocks (monzogabbro) and felsic microgranular enclaves (monzosyenite) around the Bafra (Samsun) area within Tertiary volcanic and sedimentary units of the Eastern Pontides, Northeast Turkey are described for the first time in this paper. The felsic enclaves are medium to fine grained, and occur in various shapes such as, elongated, spherical to ellipsoidal, flame and/or rounded. Most enclaves show sharp and gradational contacts with the host monzogabbro, and also show distinct chilled margins in the small enclaves, indicating rapid cooling. In the host rocks, disequilibrium textures indicating mingling or mixing of coeval mafic and felsic magmas are common, such as, poikilitic and antirapakivi textures in feldspar phenocrysts, sieve textured-patchy-rounded and corroded plagioclases, clinopyroxene megacrysts mantled by bladed biotites, clinopyroxene rimmed by green hornblendes, dissolution in clinopyroxene, bladed biotite, and acicular apatite. The petrographical and geochemical contrasts between the felsic enclaves and host monzogabbros may partly be due to a consequence of extended interaction between coeval felsic and mafic magmas by mixing/mingling and diffusion. Whole-rock and Sr-Nd isotopic data suggests that the mafic host rocks and felsic enclaves are products of modified mantle-derived magmas. Moreover, the felsic magma was at near liquidus conditions when injected into the mafic host magma, and that the mafic intrusion reflects a hybrid product formed due to the mingling and partial (incomplete) mixing of these two magmas.

Introduction

Magma mingling and mixing has become a topic of substantial interest and debate among scholars studying the evolution of igneous rocks (e.g., Eichelberger 1978; Heiken and Eichelberger 1980; Sakuyama 1981; Bacon and Metz 1984; Vernon 1983; Bacon 1986; Grove and Donnelly-Nolan 1986; Frost and Mahood 1987; Nixon and Pearce 1987; Williams and Tobisch 1994; Poli et al. 1996; Thomas and Tait 1997; Blake and Fink 2000; Eichelberger et al. 2000; De Rosa et al. 2002). According to the definitions of Bacon (1986) and Sparks and Marshall (1986), mixed magmas that are blended to form a homogenous composition are termed “mixed” or “hybrid” magmas (Macdonald et al. 2008), whereas the term “mingling” or “comingling” is used if magmas are heterogeneous physical mixtures at a microscopic or mesoscopic scale (such as banding or enclave/inclusions in the rock). The interaction between magmas in open system magma chambers has been considered responsible for a range of magmatic textures, mineral textures, and volcanic products. Included in these are schlieren (Weinberg et al. 2001), enclaves (Barbarin and Didier 1992), and a host of mineral textures (Singer et al. 1995; Robinson and Miller 1999), which are often interpreted as being the products of incomplete magma mixing, or mingling interactions.

If mafic magma is introduced before the crystallization of the felsic magma, it may result in homogeneous hybrid magmas. This type of mixing often occurs at depth and is usually favored by convection. However, if it is introduced slightly later, then the viscosities of two magmas may be sufficiently contrasting to only allow mingling. According to Sparks et al. (1977), felsic magma is quickly superheated when mixed with mafic magma, which results in increased temperature that produces a significant lowering of its viscosity. The mafic magma may also break up into blobs and

Editorial handling: L. G. Gwalani

İ. Temizel (✉)
Department of Geological Engineering, Karadeniz Technical University, TR-61080 Trabzon, Turkey
e-mail: itemizel@ktu.edu.tr

can be scattered in the felsic magma to form enclaves. The chemical mixing of mafic (host) and felsic (enclave) magma causes ion and partial mineral exchange to develop a geochemical hybrid zone, whereas the physical mingling of two melt components tends to retain the individual geochemical identities (Vernon 1983; Sparks and Marshall 1986; Barbarin and Didier 1992).

In the Eastern Pontides (Northeast Turkey), it is well documented that magma mingling and magma mixing reflect a voluminous hybridization in the genesis of the magma source of the Tertiary felsic intrusives (e.g., Boztuğ et al. 2005, 2006, 2007; Arslan and Aslan 2006; Boztuğ and Harlavan 2008). Boztuğ et al. (2005) also suggested that Eocene multi-sourced granitoids in the east-central and Eastern Pontides had been derived from hybrid magma sources resulting from the mingling and mixing of coeval mantle- and crustal-derived melts generated in a post-collisional extension-related geodynamic setting. However, small stocks of Eocene-aged mafic intrusive rocks associated with these felsic intrusive bodies are only reported as Ardeşen gabbro in the Kaçkar Batholith, and Yücedere diorite-gabbro within Dereli-Şebinkarahisar intrusives in the region (e.g., Yılmaz-Şahin et al. 2004; Boztuğ et al. 2006, 2007; Boztuğ and Harlavan 2008). The shallow seated small gabbroic stocks around the Bafra (Samsun) area at the northwestern edge of the region are described in this study for the first time that make the Miocene post-collisional mafic host rocks (MHRs) and felsic microgranular enclaves (FMEs) ideal candidates to evaluate the underlying processes of coeval mafic and felsic magma interactions. Thus, field, petrographical and geochemical works on the MHRs and FMEs present new data on and interpretations of the Tertiary hypabyssal history of the Eastern Pontides. The objectives of this study are to: (i) determine magma mixing/mingling features in the petrogenetic evolution of the MHRs and FMEs, (ii) explain the genetic linkage between the MHRs and FMEs, (iii) determine the origin and mode of formation of FMEs, and their bearing on the evolution of the magma chamber, and (iv) provide important constraints on the generation mechanisms of MHRs and FMEs.

Geological setting

The Pontides tectonic belt, which extends from northwest to northeast Turkey along the İzmir-Ankara-Erzincan suture zone (IAES) (Fig. 1a), is divided into three segments: the Western, Central, and Eastern Pontides, based on differences on pre-Jurassic basement units (e.g., Şengör and Yılmaz 1981; Okay and Şahintürk 1997; Yılmaz et al. 1997). The convergence and collision of the Tauride-Anatolide Platform (TAP) with the Eurasian plate (EP) during the closure of the north-dipping İzmir-Ankara-Erzincan ocean (IAEO) in the Late Cretaceous-Early Eocene period left several well-

documented igneous records of both the active and passive margins of this Neo-Tethyan convergence system in Turkey (Şengör and Yılmaz 1981; Bozkurt and Mittwede 2001). This collision zone between the EP and TAP migrated progressively toward the east, ranging from Santonian-Turonian in western and central Anatolia (Şengör and Yılmaz 1981; Floyd et al. 2000; Okay et al. 2001) to Palaeocene-Early Eocene (ca. 55 Ma) in the Eastern Pontides region of Turkey (Şengör and Yılmaz 1981; Okay and Şahintürk 1997; Yılmaz et al. 1997; Boztuğ et al. 2003, 2004; Arslan and Aslan 2006; Boztuğ et al. 2006; Boztuğ and Harlavan 2008).

The study area is located in Bafra (Samsun), in the northwestern edge of the Eastern Pontides (Fig. 1a and b). In the Eastern Pontides, post-collisional Tertiary aged felsic intrusive bodies (50 Ma to 40 Ma) are widespread and show compositional variation, whereas mafic intrusives are extremely limited (e.g., Yılmaz 1972; Yılmaz and Boztuğ 1996; Okay and Şahintürk 1997; Boztuğ et al. 2004; Topuz et al. 2005; Arslan and Aslan 2006; Boztuğ et al. 2006; Boztuğ and Harlavan 2008; Dokuz et al. 2006; Topuz et al. 2011). The oldest unit in the Bafra (Samsun) area is the Late Cretaceous Cankurtaran formation which is overlain conformably by the Late Cretaceous-Paleocene Akveren formation and Paleocene-Eocene-aged Atbaşı formation. These units are overlain unconformably by the Eocene-aged Kusuri formation and conformably by Middle-Late Eocene Tekkeköy formation (cf. Gedik and Korkmaz 1984; Yoldaş et al. 1985). These units are cross cut by the Miocene-aged Mahmurdağ volcanics (Gedik et al. 1984; Gedik and Korkmaz 1984) and gabbroic stocks (Fig. 2a–c). The emplacement of these volcanics and gabbroic stocks has been controlled approximately by NW-SE and/or NE-SW directed fractures. The Miocene Mahmurdağ volcanics consist of mainly basaltic-andesitic dikes and sills, flows, agglomerate and tuff. The Miocene gabbroic stocks, first described in this study, are exposed as shallow-seated small stocks and phacolith-like structures (Fig. 2a–c), and containing large augite megacrysts and felsic enclaves (Figs. 3a–f and 4a and b). One of the gabbroic stocks spreads out approximately 10 km² and has a height of 35 m (see Fig. 1b), whereas the others are 2–5 km² in width and 15–20 m in height. All these units are overlain unconformably by Quaternary old alluvium and terrace deposit, and alluvium (see Fig. 1b).

Megascopic and microscopic descriptions of rocks

Mafic Host Rock (MHR)

Several shallow-seated small gabbroic stocks exposed in the Bafra (Samsun) area contain numerous felsic microgranular enclaves (FMEs) found within mafic host rocks (MHRs) (see

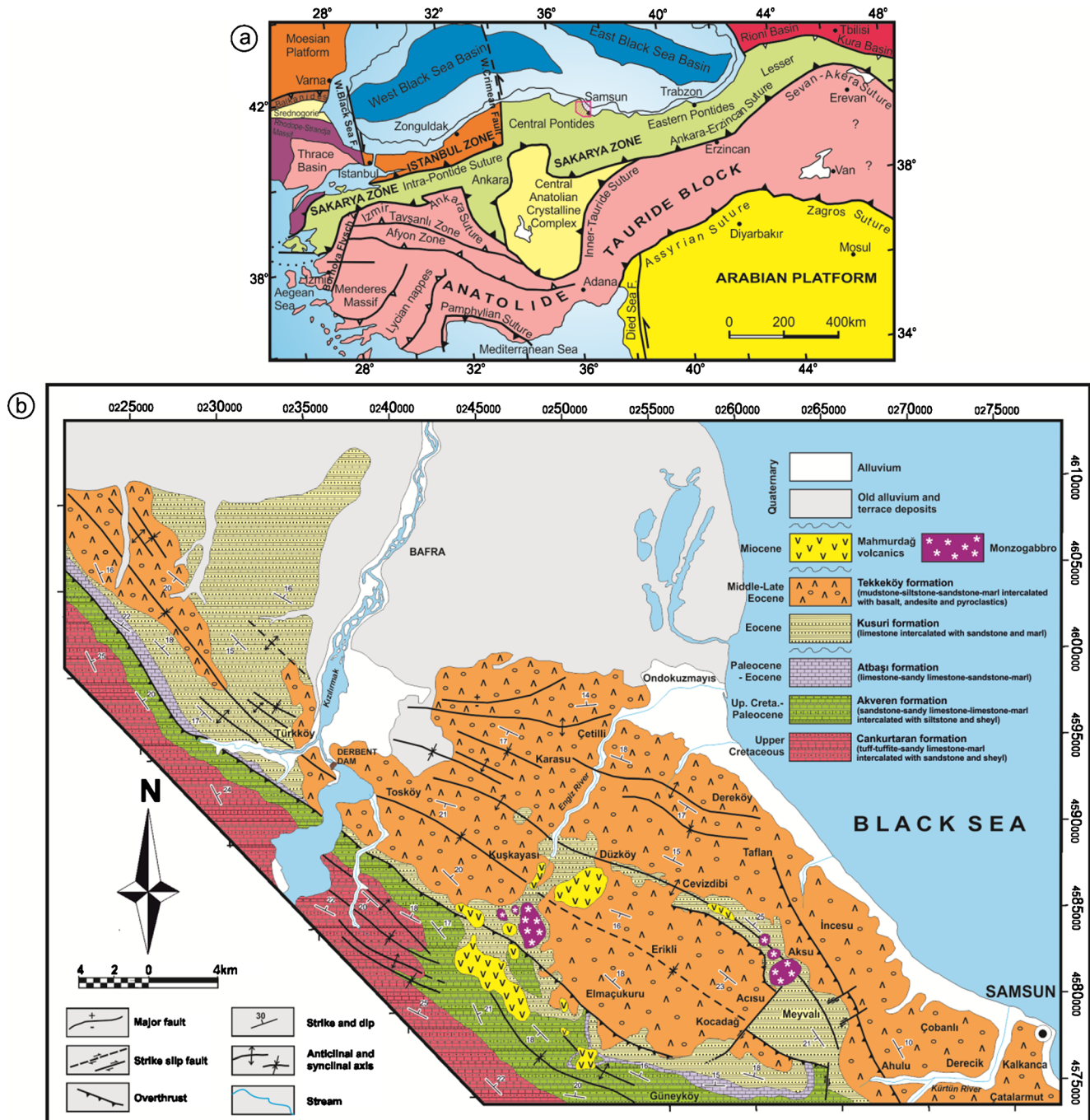


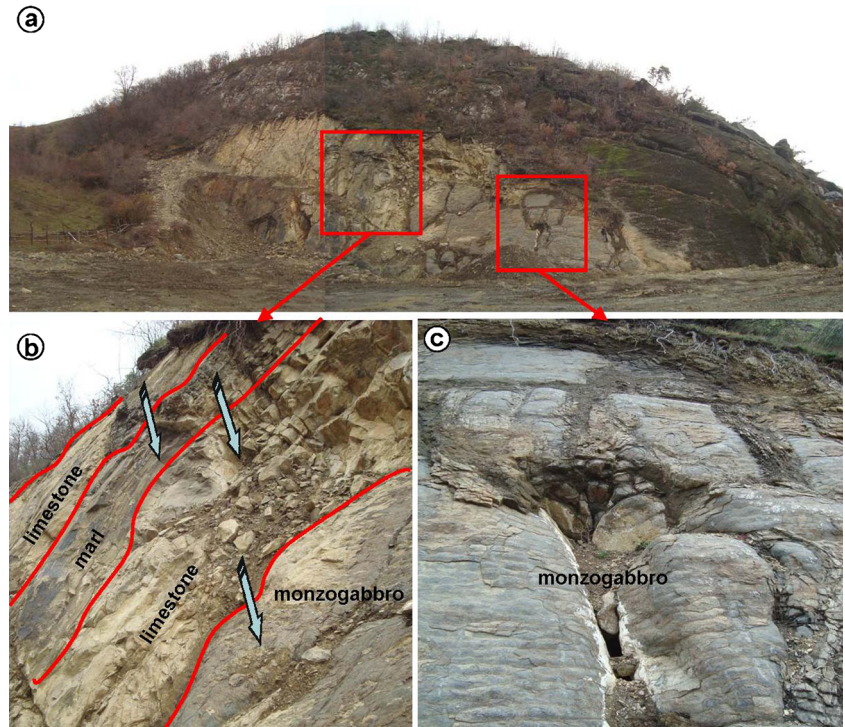
Fig. 1 **a** Tectonic map of north-eastern Mediterranean region showing the major sutures and continental blocks. Sutures are shown by heavy lines with the polarity of former subduction zones indicated by filled triangles. Heavy lines with open triangles represent active subduction zones. Small open triangles indicate the vergence of the major fold and

thrust belts (modified after Okay and Tüysüz 1999), **b** simplified geological map of the Bafra (Samsun) area (modified after Yoldaş et al. 1985; Güven 1993), showing the distribution of the studied intrusive stocks

Fig. 3a–f). The mafic host rocks are predominantly monzogabbroic in composition. Monzogabbro is dark-gray in color and mostly coarse-grained. In general, coarse-grained monzogabbro has phaneritic, hypidiomorphic inequigranular, and sometimes porphyritic textures (Fig. 4a and b), and has a simple mineralogical composition. Essentially it contains

phenocrysts of plagioclase, alkali feldspar, clinopyroxene, olivine, biotite, hornblende, Fe-Ti oxide, and to a lesser extend accessory apatite and sphene. In addition, rare natrolite type zeolite occurrences as void- and micro crack- infillings (Yağcıoğlu et al. 2012) are also observed at the contact of monzogabbro and felsic microgranular enclaves. A poikilitic

Fig. 2 Field photographs from MHRs illustrating **a** phacolith-like structure, **b** contact between limestone-marl intercalation and MHR, and **c** grey and dark grey colored MHR

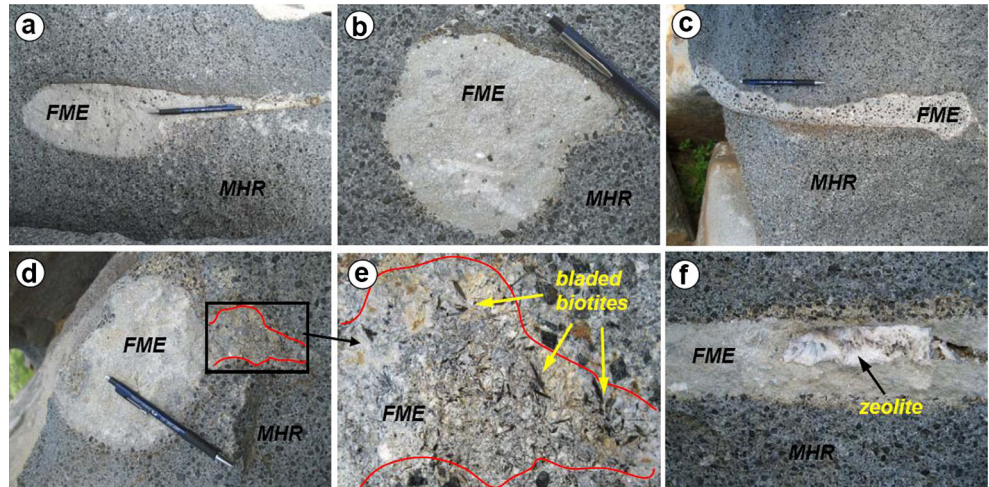


texture (Fig. 4d and g) is characteristic in several host rock samples containing large euhedral-subhedral plagioclase and/or alkali feldspar phenocrysts up to 3.0 mm in size, with the inclusion of subhedral clinopyroxene, biotite, hornblende, and Fe-Ti oxide.

Euhedral to subhedral plagioclase represents the dominant mineral phase. Plagioclases are generally anti-rapakivi and sieved-textured with a resorption zone, resorbed core, and oscillatory zoning. The plagioclase phenocrysts also display multiple zoning of repeated discontinuous zones. Intergrowths and overgrowths of multiple and continuously zoned plagioclase, respectively, occur along discrete dissolution surfaces. Rectangular plagioclase also has variable

degrees of sericitization, particularly in its core. The alkali feldspar oikocrysts ranging from 2 mm to 5 mm in size are identical to those in the host rocks, they also show slightly perthitic, anti-rapakivi and poikilitic textures (Fig. 4d). Clinopyroxenes, which vary in shape from euhedral to subhedral crystals, are mainly present both as megacrysts and phenocrysts, usually with resorption features. Specifically, clinopyroxene megacrysts up to about 5.0 mm in size are the most abundant ferromagnesian mineral phase in the host rocks (Fig. 4g and h). They exhibit oscillatory and sector zoning, or are rounded, broken or twinned, embayed, and have signs of dissolution. In a few samples, clinopyroxene can be found as overgrowth rims on earlier-formed plagioclase crystals. Relic

Fig. 3 Macrophotos of felsic microgranular enclaves (FMEs, monzosyenite), having various shapes as elongated spherical and ellipsoidal (**a**), rounded or lobate (**b**, **d**), planar or flame (**c**) irregular forms and ranging from a few centimeters to one meter in size and from 5 cm to 20 cm in diameter in the mafic host rock (MHR, monzogabbro), **e** bladed biotites situated across the contacts between MHR and FME, and **f** zeolite as void- and micro crack- infillings in the FME



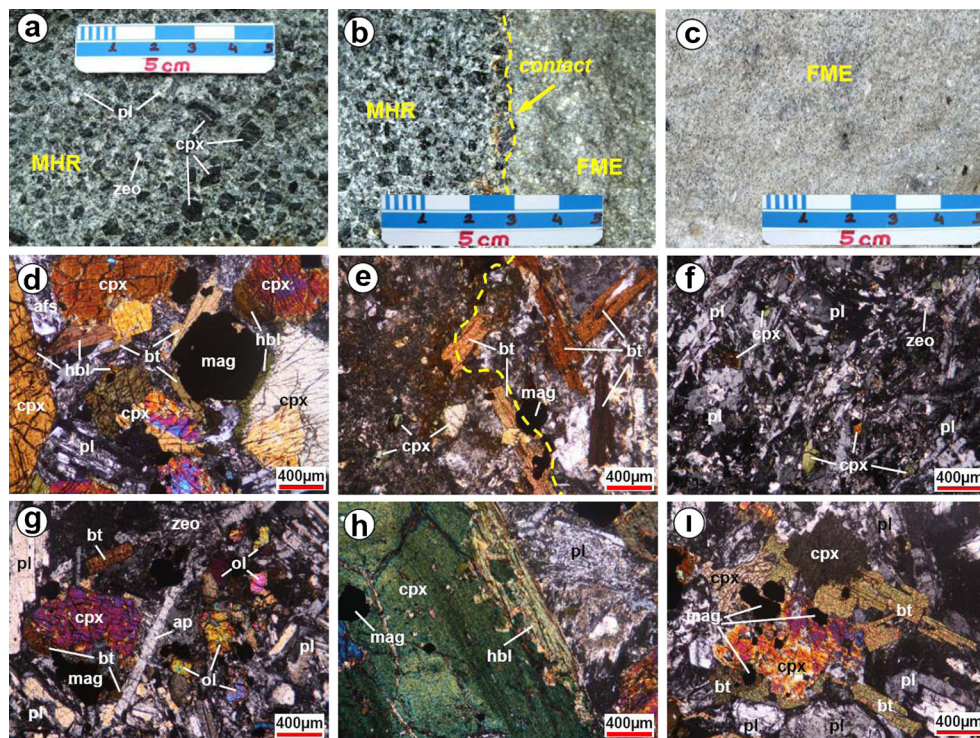


Fig. 4 Macrophotos of the **a** monzogabbro (MHR), **b** contact between monzogabbro (MHR) and enclave (FME), and **c** monzosyenite (FME). Microphotographs (d-i) of disequilibrium textures indicating mingling/mixing of mafic and felsic magmas: **d** poikilitic textures in alkali feldspar phenocryst including clinopyroxene, biotite, hornblende and magnetite in the MHR (Sample No: B-50; xpl), **e** clinopyroxene, bladed biotite and complex resorption textured plagioclase in the chilled and/or sharp contact of MHR with FME (Sample No: B-17; xpl), **f** sieve, boxy cellular and complex resorption textured plagioclases, clinopyroxene and zeolite in the

FME (Sample No: B-17; xpl), **g** biotite, olivine, embayed clinopyroxene and acicular apatite in the MHR (Sample No: B-17; xpl), **h** oscillatory and sector zoned clinopyroxene megaacryst rimmed by green hornblende and spongy-textured plagioclase with resorption zone in the MHR (Sample No: B-50; xpl), **i** clinopyroxene mantled by bladed biotites and sieve textured-patchy-rounded and corroded plagioclases in the MHR (Sample No: B-36; xpl). Symbols for minerals: pl, plagioclase; afs, alkali feldspar; cpx, clinopyroxene; hbl, hornblende; bt, biotite; ol, olivine; mag, magnetite; zeo, zeolite; ap, apatite

clinopyroxene crystals also occur in a large number of hornblende grains (Fig. 4h).

Olivine phenocrysts are typically unzoned, subhedral-anhedral, and fractured. Olivines are slightly altered to red-brown iddingsite, and are present in trace amounts in the host rocks (Fig. 4g). Biotite is the most abundant of the mafic minerals after clinopyroxene (Fig. 4e, g and i). This phase occurs as orange-brown, weakly pleochroic, and/or red-brown to yellow, pleochroic grains. Biotites are typically flaky, and contain inclusions of iron-titanium oxide and olivine. Red-brown bladed biotites ranging in size from 0.5 mm to 3 mm are abundant, and are mostly found next to the contact of the enclaves and the host rocks (Fig. 4e), whereas small (0.2 mm to 0.5 mm) randomly oriented biotite grains often form 2-mm long aggregates, and are found around Fe-Ti oxides in the enclaves and host rocks. Green or olive green to pale yellow hornblende occurs as anhedral to subhedral 0.5 mm to 2.0 mm grains, as rims on clinopyroxene phenocrysts showing sector and normal zoning. The larger iron-titanium oxide grains occur in association with biotite (Fig. 4d), whereas the small anhedral round grains occur as inclusions in clinopyroxene

and plagioclase, and randomly scattered throughout the sample in the intergrowths formed by biotite breakdown (Fig. 4i). Apatite has a typical acicular shape (Fig. 4g), and typically occurs in clots as stubby grains of about 1 mm, and is occasionally included in clinopyroxene and plagioclase. Sphene is typically anhedral to subhedral, although several euhedral grains exist as diamond-shaped crystals of extremely high relief with a brown or red-brown color of less than 0.2 mm to 0.5 mm.

Felsic Microgranular Enclave (FME)

Field measurements, such as orientations and dimensions, are focused on the fine- to medium-grained felsic microgranular enclaves. These are the largest, most abundant, and most easily observed enclaves in the mafic host rocks. Although numerous FMEs in the study area are planar, elongated spherical, and ellipsoidal, certain FMEs have wavy, flame, rounded, or lobate irregular forms, ranging from a few centimeters to one meter in size, and from 5 cm to 20 cm in diameter (see Fig. 3a-f). Two-dimensional horizontal exposures of enclaves

indicate that a large number of them have a bow or bulge on one side. Some ellipses have wispy projections into the mafic host rock. Most enclaves show pervasive sharp contacts with the host monzogabbro, and distinct chilled margins especially in the small enclaves indicating rapid cooling after entering the mafic host magma. Additionally, the contacts between the enclaves and host rocks are also occasionally gradational and show no reaction or cooling zones. Bladed biotite phenocrysts are only found across these contacts between the mafic host rocks and FMEs (see Fig. 3d and e). FMEs are generally medium to fine-grained with hypidiomorphic equigranular texture, and are monzosyenite in composition. FMEs are extremely light colored (Fig. 4b and c) relative to those of mafic host rocks; they mainly consist of plagioclase, alkali feldspar, clinopyroxene, biotite, hornblende, and Fe-Ti oxides; and have an almost identical mineral assemblage to their host rocks. In addition, rare sericitization and zeolitization are observed. In a number of FMEs, natrolite and quartz are common as void- and micro-crack infillings (see Fig. 3f).

Plagioclase represents the dominant mineral phases. Albite and albite-carlsbad twinnings are characteristic of the plagioclase, which may have sieve and boxy cellular textures (Fig. 4e and f). Occasionally, plagioclase is euhedral to subhedral, and displays patchy zoning and complex resorption textures. The alkali feldspar phenocrysts are anhedral to subhedral, and exhibit resorption. Elongated plagioclase crystals may be aligned within granular clinopyroxene and biotite and intergranular Fe-Ti oxides. Mafic minerals are a minor component of the felsic enclaves (Fig. 4e and f). Biotite is the dominant mafic phase, and it occurs as small rounded, subhedral to anhedral red-brown, golden brown, to yellow grains. Other mafic phases include clinopyroxene, hornblende, and Fe-Ti oxides. Clinopyroxene occurs in several samples as small rounded anhedral to elongated ovoid grains. Mafic minerals do not exceed 1 mm and are typically less than 0.5 mm (Fig. 4e and f). Fe-Ti oxides are less abundant in the FMEs relative to their mafic host rocks.

Analytical method

A total of 35 samples were collected from gabbroic stocks and their felsic microgranular enclaves and from the contacts, for understanding the behavior of magma mixing and mingling. Based on the petrographical studies, the fresh and most representative rock samples were analyzed for whole-rock major, trace-, and rare-earth-element, and Sr-Nd isotopic compositions.

Whole-rock petrochemical analyses were carried out at the ACME Analytical Laboratories Ltd. in Vancouver, Canada. Major and trace element compositions were determined by ICP-AES after 0.2 g samples of rock powder were fused with 1.5 g LiBO₂, and then dissolved in 100 ml 5 % HNO₃. Rare

earth element contents were analyzed by ICP-MS after 0.25 g samples of rock powder were subjected to acid treatment. Loss on ignition (LOI) is calculated by the weighted difference after subjecting the samples to ignition of ~1,000 °C. Detection limits range from 0.002 wt % to 0.04 wt % for major oxides, 0.1 ppm to 8 ppm for trace elements, and from 0.01 ppm to 0.3 ppm for the rare earth elements (Table 1).

Sr and Nd isotopic compositions for five samples were also analyzed at the Pacific Centre for Isotopic and Geochemical Research (PCIGR) of the University of British Columbia in Canada. For isotopic analysis, the samples were repeatedly leached with HCl of 6 N to remove secondary alteration. Sr and Nd were separated using the method described by Weis et al. (2006). Isotope ratios were measured by a Thermo Finnigan Triton Thermal Ionization Mass Spectrometry (TIMS) in static mode with relay matrix rotation on single Ta filament and double Re-Ta filament for Sr and Nd isotopic analyses, respectively. During the analyses, the NBS987 Sr standard showed an average of 0.710240±0.000013, and the La Jolla Nd standard showed an average value of 0.511857±0.000017.

Whole-rock and Sr-Nd isotope geochemistry

Whole-rock major oxide, trace-, rare earth- elements, and Sr-Nd isotope data on the MHRs and FMEs from the Bafra (Samsun) area are presented in Tables 1 and 2, respectively. The chemical classification and nomenclature of the studied MHR, FME and contact samples were not successfully achieved in various plots due to sericitization and zeolitization (especially in FMEs), which might cause an increase in alkalinity. The MHR, FME and contact samples have loss on ignition (LOI) as 2.0–3.6 wt%, 4.9–5.4 wt.% and 3.9–4.1 wt.%, respectively (see Table 1). Thus, the samples plot in the foid-gabbro field for MHRs, in the foid-monzosyenite field for the FMEs, and in the foid-monzdiorite field for the contact samples (Fig. 5a) using the TAS (total alkali silica) diagram of Middlemost (1994). For this reason, the immobile trace element based Nb/Y versus Zr/Ti (Fig. 5b) diagram of Pearce (1996) was also accounted, and the samples are classified as basalt (i.e., gabbro) for the MHRs, trachyte (i.e., syenite) for the FMEs, and andesite/basalt (i.e., diorite/gabbro) for the contact samples. The samples show calc-alkaline characteristics on both the AFM (Na₂O+K₂O-FeO(t)-MgO)(Fig. 6a) diagram of Irvine and Baragar (1971) and the Ce/Yb versus Ta/Yb (Fig. 6b) diagram of Pearce (1982). The alkalinity of the samples, as measured by the agpaitic index [AI=mol (Na+K)/AI], is indicated as a function of SiO₂ (Fig. 6c). The agpaitic index shows that all samples are predominantly calc-alkaline (AI<0.87; Liégeois and Black 1987). The alumina saturation index (i.e., A/CNK=molar Al₂O₃/CaO+Na₂O+K₂O) of granitoids has been commonly used to distinguish between

Table 1 Whole-rock major (wt.%), trace (ppm) and rare earth element (ppm) analyses of MHR, FME and contact samples from the Bafra (Samsun) area

Sample no.:	dl	MHR (monzogabbro)						Contact samples			FME (monzosyenite)			
		B-17	B-36	B-39	B-50	B-51	B-55	CHM-1	CHM-2	GRM-1	A-2	A-4	A-5	A-6
SiO ₂	0.01	43.54	43.79	43.71	42.91	42.50	43.68	46.44	47.44	50.87	53.91	54.17	54.26	53.58
TiO ₂	0.01	0.93	0.93	0.94	0.97	1.03	0.90	0.70	0.61	0.43	0.13	0.13	0.13	0.12
Al ₂ O ₃	0.01	16.32	16.36	16.32	16.61	15.76	16.61	17.56	18.24	18.32	20.97	20.61	20.69	21.02
Fe ₂ O ₃ (t)	0.04	12.43	12.24	12.57	12.44	12.96	11.88	9.91	9.01	6.71	3.99	3.84	3.76	3.95
MnO	0.01	0.24	0.24	0.25	0.26	0.26	0.24	0.21	0.20	0.16	0.13	0.12	0.12	0.13
MgO	0.01	5.31	5.52	5.46	5.21	5.67	5.14	3.88	3.40	2.70	0.45	0.41	0.44	0.39
CaO	0.01	12.02	12.56	12.46	14.06	14.96	11.71	9.03	7.95	6.13	2.70	2.49	2.47	2.11
Na ₂ O	0.01	2.29	2.35	2.25	2.29	2.01	2.58	4.94	5.31	5.56	7.29	7.44	7.45	7.72
K ₂ O	0.01	2.87	2.75	2.60	2.19	1.89	2.76	2.74	3.19	4.64	5.36	5.33	5.31	5.34
P ₂ O ₅	0.01	0.51	0.51	0.49	0.45	0.54	0.48	0.37	0.34	0.12	0.05	0.07	0.08	0.07
LOI	0.01	3.20	2.30	2.60	2.20	2.00	3.60	3.90	4.00	4.10	4.90	5.30	5.20	5.40
Total	0.01	99.66	99.55	99.65	99.59	99.58	99.58	99.68	99.69	99.74	99.88	99.91	99.91	99.83
Zr	0.1	75.8	80.5	79.8	91.8	100.6	89.3	142.1	150.7	178.2	236.9	235.0	245.4	245.7
Y	0.1	21.6	23.6	23.3	28.1	31.3	23.1	26.7	24.7	21.3	25.0	21.6	23.8	20.6
Sr	0.5	917.7	917.4	981.4	1032.8	1027.8	962.7	660.2	617.6	369.2	294.0	271.4	288.5	259.5
Rb	0.1	52.0	60.2	52.6	29.9	26.3	55.3	42.5	46.9	73.2	76.3	75.8	74.7	74.6
Th	0.2	4.1	4.3	3.8	5.3	4.5	4.6	9.7	10.3	13	19.0	17.3	18.6	18.3
Ta	0.1	0.3	0.3	0.3	0.4	0.4	0.3	0.6	0.5	0.5	1.0	0.8	1.0	0.8
V	8.0	348	363	362	381	414	328	240	201	134	16	24	14	10
Pb	0.1	6.5	5.5	6.1	4.5	4.1	5.3	9	9.2	8.5	10.7	10.9	10.7	12.3
Ni	0.1	7.0	9.0	12.4	6.3	8.2	8	5.1	4.9	3.5	0.7	1.0	0.9	1.7
Co	0.2	39.3	41.9	44.1	41.3	45.1	37.5	28.9	26	17.3	5.8	5.5	5.3	4.8
Cr	20	20	50	70	20	20	40	20	50	30	bdl	bdl	bdl	bdl
Ba	1.0	731	785	708	786	678	774	550	569	623	378	352	372	349
Nb	0.1	4.3	4.8	5.1	5.4	5.4	4.8	7.6	8.2	7.5	12.4	14.9	16.8	13.1
Hf	0.1	2.5	2.5	2.8	2.5	2.8	2.5	3.7	3.9	3.6	5.2	4.7	4.9	5.4
La	0.1	19.3	20.9	20.5	25.6	25.0	21.7	27.9	29.4	28.2	38.2	37.3	38.8	38
Ce	0.1	44.6	42.7	43.1	54.1	55.1	42	52.5	53.7	52.3	65.0	66.9	68.3	65.4
Pr	0.02	5.46	5.79	5.44	7.19	7.34	5.6	6.33	6.19	5.75	7.02	6.72	7.14	6.96
Nd	0.3	22.7	25.9	22.3	31.7	33.1	22.6	25.9	23.1	21.2	24.2	21.6	24.0	23.2
Sm	0.05	5.29	5.72	5.78	6.56	7.05	5.33	5.12	4.84	4.57	4.34	4.07	4.53	4.22
Eu	0.02	1.46	1.68	1.58	1.86	2.00	1.54	1.29	1.19	1.04	0.83	0.76	0.82	0.83
Gd	0.05	5.03	5.73	4.99	5.99	6.57	5.18	4.82	4.77	4	3.69	3.26	3.31	3.38
Tb	0.01	0.75	0.85	0.85	0.97	1.01	0.73	0.76	0.73	0.64	0.67	0.61	0.66	0.57
Dy	0.05	4.19	4.62	4.10	5.36	5.51	4.42	3.93	4.47	4.25	4.18	3.38	3.72	3.48
Ho	0.02	0.80	0.86	0.90	1.07	1.06	0.81	0.96	0.85	0.81	0.89	0.84	0.81	0.77
Er	0.03	2.22	2.41	2.56	2.95	3.01	2.34	2.84	2.64	2.45	2.89	2.69	2.65	2.38
Tm	0.01	0.34	0.38	0.37	0.43	0.45	0.36	0.45	0.42	0.46	0.50	0.49	0.51	0.43
Yb	0.05	2.18	2.45	2.55	3.06	2.95	1.93	2.93	3.09	2.65	3.35	3.49	3.51	3.47
Lu	0.01	0.30	0.34	0.36	0.39	0.42	0.34	0.4	0.46	0.45	0.55	0.54	0.59	0.51
Eu _N /Eu [*]	0.86	0.90	0.90	0.91	0.90	0.90	0.79	0.76	0.74	0.63	0.64	0.65	0.67	
La _N /Lu _N	6.68	6.38	5.91	6.81	6.18	6.63	7.24	6.64	6.51	7.21	7.17	6.83	7.74	
La _N /Yb _N	5.98	5.76	5.43	5.65	5.73	7.60	6.43	6.43	7.19	7.71	7.22	7.47	7.40	
Mg#	29.9	31.1	30.3	29.5	30.4	30.2	28.1	27.4	28.7	10.1	9.6	10.5	9.0	
A/CNK	0.59	0.57	0.58	0.56	0.53	0.59	0.58	0.60	0.59	0.66	0.65	0.65	0.66	
A/NK	1.52	1.53	1.60	1.73	1.88	1.47	1.01	0.96	0.83	0.75	0.73	0.73	0.73	

Table 1 (continued)

dl	MHR (monzogabbro)						Contact samples			FME (monzosyenite)			
	B-17	B-36	B-39	B-50	B-51	B-55	CHM-1	CHM-2	GRM-1	A-2	A-4	A-5	A-6
Sample no.:													
A.I.	0.19	0.21	0.21	0.26	0.25	0.23	0.47	0.45	0.33	0.43	0.43	0.43	0.45

$\text{Fe}_2\text{O}_3(\text{t})$: total iron as Fe_2O_3 ; LOI: loss on ignition. Mg# (Mg-number) = $100 \times \text{MgO}/(\text{MgO} + \text{Fe}_2\text{O}_3(\text{t}))$. Symbols: bdl: below detection limit, dl: detection limit. A/CNK = $\text{Al}_2\text{O}_3/(\text{CaO} + \text{Na}_2\text{O} + \text{K}_2\text{O})$, A/NK = $\text{Al}_2\text{O}_3/(\text{Na}_2\text{O} + \text{K}_2\text{O})$, A.I. (Agpaitic Index) = $[\text{Na}^+/\text{Al}]$

metaluminous (I-type, A/CNK < 1.05) and peraluminous (S-type, A/CNK > 1.05) granitoids (Chappell and White 1974). On the A/CNK versus SiO_2 (wt.%) diagram of Chappell and White (1974), the MHR, FME and contact samples have A/CNK molecular ratios as 0.53–0.59, 0.65–0.66 and 0.58–0.60, respectively (see Table 1), which dominantly suggests a metaluminous character (Fig. 6d).

Most major oxide and trace element variations exhibit well-defined positive or negative correlations with increasing SiO_2 content (Fig. 7), reflecting the significant effect of fractional crystallization processes of different mineral phases during the evolution of the studied rocks. An increase in the SiO_2 content of MHR, FME and contact samples brings a corresponding decrease in CaO , P_2O_5 , TiO_2 , MnO , $\text{Fe}_2\text{O}_3(\text{t})$, MgO , Sr , Ba , V , and Co content and an increase in Al_2O_3 , K_2O , Na_2O , Rb , Hf , Zr , Nb , and Th content (Fig. 7). A decrease in P_2O_5 , TiO_2 , and Sr content corresponding to an increase in SiO_2 content is probably related to apatite, Fe-Ti oxide, and plagioclase fractionation, respectively. CaO decreases with increasing SiO_2 , reflecting clinopyroxene and plagioclase fractionation. Fractionation of alkali feldspar also reduces Ba and Sr . An increase in K_2O and Rb content corresponding to an increase in silica content is consistent with the late appearance of alkali feldspar and biotite in the crystallization sequence. $\text{Fe}_2\text{O}_3(\text{t})$ decreases with increased differentiation, a pattern probably related to clinopyroxene fractionation. A decrease in $\text{Fe}_2\text{O}_3(\text{t})$, MgO , and MnO content corresponding to an increase in SiO_2

content is probably related to hornblende and biotite fractionation in MHR, FME and contact samples. High MgO and CaO content, low SiO_2 content, and Mg# relative to those of FMEs and the contrasting behavior of these elements when plotted against silica concentrations suggest that magmas for MHRs were generated by olivine and clinopyroxene fractionation. Lower values of Mg# in FMEs may also reflect the greater importance of hornblende and the lower importance of Fe-Ti oxide in the crystallization assemblage; crustal assimilation may also have some effect. All these variations can be explained by the fractionation of common mineral phases as clinopyroxene + plagioclase + biotite ± hornblende ± olivine ± Fe-Ti oxide ± apatite in MHRs and biotite + plagioclase ± alkali feldspar ± Fe-Ti oxide in FMEs.

The primitive mantle-normalized (Sun and McDonough 1989) multi-element variation diagrams of the MHR, FME and contact samples in Fig. 8a are similar to those of subduction-related magma (Pearce et al. 1990; Pearce and Peate 1995) with enrichment in large-ion lithophile elements (LILEs; e.g., Rb , Ba , Sr , and K_2O) relative to high-field strength elements (HFSEs; i.e., Nb , Zr , Y , and TiO_2) and heavy rare earth elements (HREEs; i.e., Yb and Lu). All samples show a prominent Nb-Ta trough (Fig. 8a). Although negative anomalies of Nb and other HFSEs relative to LILE might be related to crustal contamination, they are characteristic features of subduction-related magma, and a result of the relative enrichment of mantle source through the addition of LILEs from the subducting slab

Table 2 Sr and Nd isotopic analyses of MHR and FME samples from the Bafra (Samsun) area

Sample	Rb (ppm)	Sr (ppm)	Sm (ppm)	Nd (ppm)	$^{87}\text{Rb}/^{86}\text{Sr}$	$^{87}\text{Sr}/^{86}\text{Sr}$	$(\pm 2\sigma_m)$	$^{147}\text{Sm}/^{144}\text{Nd}$	$^{143}\text{Nd}/^{144}\text{Nd}$	$(\pm 2\sigma_m)$	$\varepsilon\text{Nd}_{(0)}$	T_{DM}^* (Ga)
Mafic Host Rock (MHR, Monzogabbro)												
B-17	52.0	917.7	5.30	22.7	0.1639	0.704655	(07)	0.1412	0.512714	(06)	1.48	0.86
B-36	60.2	917.4	5.72	25.9	0.1898	0.704700	(07)	0.1335	0.512725	(06)	1.69	0.76
B-50	29.9	1032.8	6.56	31.7	0.0837	0.704942	(07)	0.1251	0.512669	(07)	0.60	0.78
Felsic Microgranular Enclave (FME, Monzosyenite)												
A-2	76.3	294.0	4.34	24.2	0.7507	0.705193	(07)	0.1084	0.512717	(07)	1.54	0.60
A-4	75.8	271.4	4.07	21.6	0.8079	0.705241	(07)	0.1139	0.512716	(07)	1.52	0.63

Uncertainties for the $^{87}\text{Sr}/^{86}\text{Sr}$ and $^{143}\text{Nd}/^{144}\text{Nd}$ ratios are $2\sigma_m$ errors in the last two digits (in parentheses). $\varepsilon\text{Nd}(0)$ values are calculated relative to CHUR with present-day values of $^{143}\text{Nd}/^{144}\text{Nd} = 0.512638$ (Jacobsen and Wasserburg 1980). Nd single-stage model ages (T_{DM}^*) are calculated with a depleted-mantle reservoir and present-day values of $^{143}\text{Nd}/^{144}\text{Nd} = 0.513151$ and $^{147}\text{Sm}/^{144}\text{Nd} = 0.219$ (Liew and Hofmann 1988)

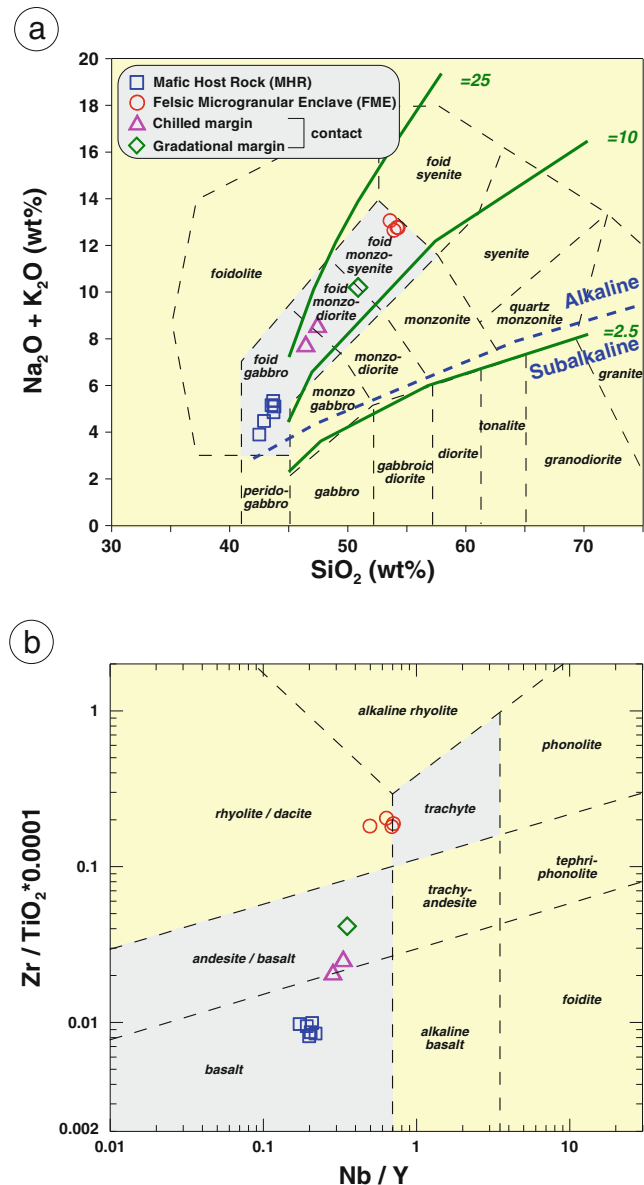


Fig. 5 Chemical classification and nomenclature plots of the MHR, FME and contact samples from the Bafraya (Samsun) area using **a** the total alkalis vs. silica (TAS) diagram (after Middlemost 1994) (σ is a Rittmann index $[(K_2O+Na_2O)^2/(SiO_2-43)]$, separate the alkaline and subalkaline fields of Miyashiro (1978)) and **b** Nb/Y vs. Zr/Ti diagram (after Pearce 1996)

to the mantle (McCulloch and Gamble 1991; Borg et al. 1997). Trace element variations in MHR, FME and contact samples with high LILE–HFSE ratios are mostly similar, although FMEs have more significantly depleted P_2O_5 and TiO_2 content and more enriched Pb content than MHRs (Fig. 8a), implying a similar magma source(s) for MHRs and FMEs.

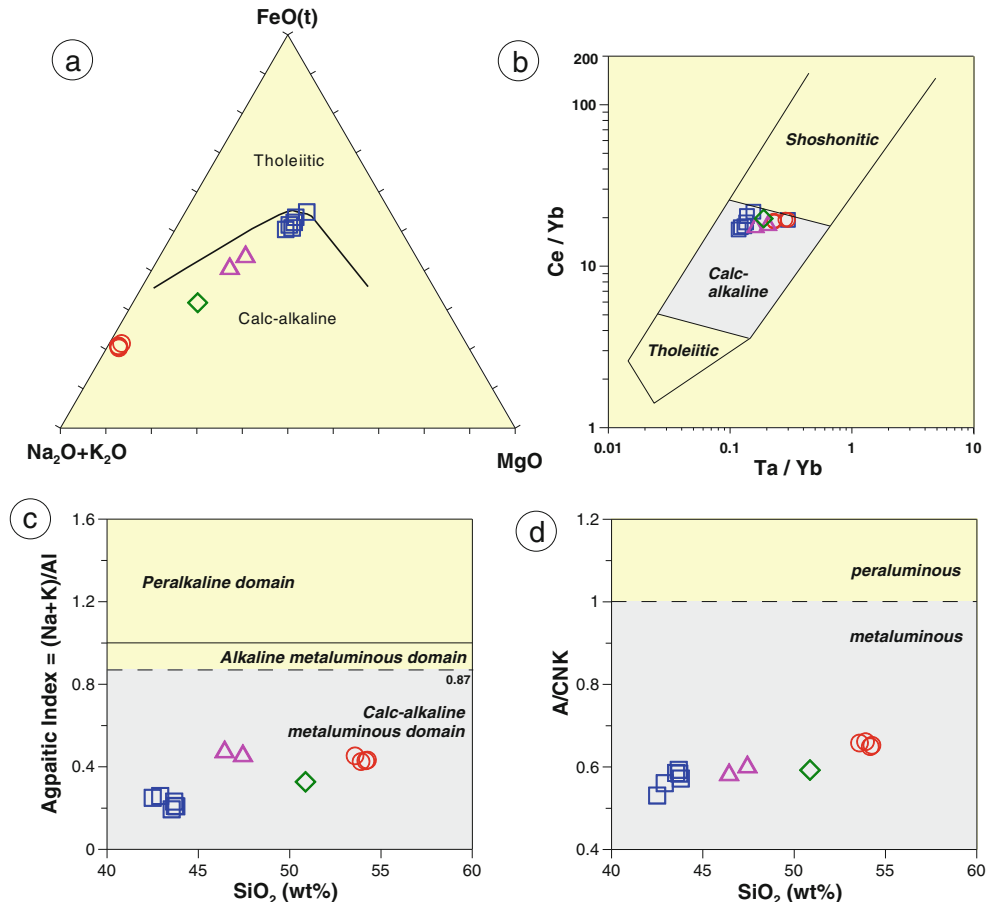
As for chondrite-normalized (Taylor and McLennan 1985) rare earth element (REE) patterns (Fig. 8b), MHR, FME and contact samples have high total REE content and are rich in light rare earth elements (LREEs) relative to HREEs. MHR,

FME and contact samples show moderately fractionated chondrite-normalized REE patterns subparallel to each other with La_N/Lu_N of 5.91–6.81, 6.83–7.74 and 6.51–7.24 for MHR, FME and contact samples, respectively, indicating the same or a similar source region for mafic and felsic rocks. Moreover, MHR, FME and contact samples are extremely rich in LREEs (La of 53–70, 102–106 and 76–80 times that of chondrite for MHR, FME and contact samples, respectively) relative to chondrite, but are less rich in HREEs (Yb of 9–12, 13–14 and 11–12 times that of chondrite for MHR, FME and contact samples, respectively), resulting in La_N/Yb_N ratios of 5.43–7.60, 7.22–7.71 and 6.43–7.19, respectively (Fig. 8b). REE distributions also have characteristic concave patterns in MHR, FME and contact samples that tend to flatten toward LREEs and HREEs, suggesting the significant effect of clinopyroxene and/or hornblende fractionation (Gill 1981; Thirlwall et al. 1994) on the evolution of the rocks studied (Fig. 8b). FMEs have strongly negative Eu anomalies (mean $Eu_N/Eu^*=0.63–0.67$) probably associated with plagioclase fractionation, whereas MHR and contact samples exhibit no or slight negative Eu anomalies (mean $Eu_N/Eu^*=0.86–0.91$ and 0.74–0.79, respectively), suggesting insignificant plagioclase fractionation or high oxygen fugacity (Fig. 8b). Under high fO_2 (oxygen fugacity) conditions, Eu is present in the form of Eu^{3+} , which is not incorporated into plagioclase. High magmatic water content, as evidenced by abundant hornblende and biotite phenocrysts, suppresses plagioclase crystallization until the later stages of fractionation and results in the absence of negative Eu anomalies. These processes may explain the absence of any significant Eu anomaly in these MHR and contact samples.

MHRs have a $^{87}Sr/^{86}Sr$ ratio (0.7047–0.7049) and a $^{143}Nd/^{144}Nd$ ratio (0.51267–0.51273) corresponding to ε_{Nd} values between 0.60 and 1.69 (Table 2). FMEs have a $^{87}Sr/^{86}Sr$ ratio (0.7052) and a $^{143}Nd/^{144}Nd$ (0.51272) ratio corresponding to ε_{Nd} values between 1.52 and 1.54 (Table 2). The corresponding Nd single-stage model ages (T_{DM}) of MHRs and FMEs are 0.76 Ga to 0.86 Ga and 0.60 Ga to 0.63 Ga, respectively. These Nd-depleted mantle model (T_{DM}) ages suggest that the lithospheric mantle source for MHRs and FMEs rocks is Neo-Proterozoic (0.76–0.86 Ga and 0.60–0.63 Ga, respectively) in age, similar to the subcontinental lithospheric mantle (SCLM) source of post-collisional volcanic rocks in the Eastern Pontides (e.g., Arslan et al. 2013).

Tectono-magmatic discrimination diagrams are used here to interpret the tectonic setting of MHR, FME and contact samples from Bafraya area. In the Rb (ppm) vs. Y+Nb (ppm) and Ta (ppm) vs. Yb (ppm) diagrams of Pearce et al. (1984) (Fig. 9a and b, respectively), all samples plot exclusively in the post-collisional volcanic arc granite field, supporting emplacement in subduction-related settings as already inferred from their rich LREE–LILE and depleted HFSE

Fig. 6 **a** AFM ternary diagram (tholeiitic-calcalkaline dividing curve is from Irvine and Baragar 1971), **b** Ce/Yb vs. Ta/Yb diagram (after Pearce 1982), **c** agpaitic index ($AI = \frac{Na+K}{Al}$) vs. SiO_2 (wt.%) diagram showing the alkaline to peralkaline characters (the dash line with $AI = 0.87$ after Liégeois and Black 1987) and **d** molar ratios $Al_2O_3/(CaO+Na_2O+K_2O)$ (A/CNK) vs. SiO_2 (wt%) diagram (after Chappell and White 1974) for the MHR, FME and contact samples from the Bafraya (Samsun) area (symbols are as in Fig. 5a)



characteristics. In Fig. 9c (Harris et al. 1986), MHR, FME and contact samples plot in the volcanic arc field. FME and contact samples with such characteristics can be plotted in the diagram Eby (1992) (Fig. 9d), which distinguishes A1-type granitoids, produced by fractional crystallization of mantle material, from A2-type granitoids with strong crustal contamination. The studied samples plot in the A2-type granitoid field (Fig. 9d), supporting emplacement in late post-collisional settings (e.g., Best 2006).

Discussion

Petrogenetic consideration of mafic and felsic magmas

According to geochemical evidence, the parent magma of MHRs and FMEs was formed by the melting of lithospheric mantle material enriched by subduction-induced fluids. MHRs and FMEs plot in the partly depleted quadrant of a conventional Sr vs. Nd isotope diagram, where they overlap the field defined by Eastern Pontides Tertiary volcanics (Fig. 10a) (Kaygusuz et al. 2011; Temizel et al. 2012; Arslan et al. 2013; Aslan et al. 2013). Moreover, the Sr and Nd isotopic

composition of MHRs and FMEs is relatively homogeneous with $^{87}Sr/^{86}Sr$ of 0.7047–0.7052, $^{143}Nd/^{144}Nd$ of 0.51267–0.51272 and $\varepsilon_{Nd(0)}$ values of +0.60 to +1.69. A narrow range of $^{87}Sr/^{86}Sr$ ratios and positive $\varepsilon_{Nd(0)}$ values of MHRs and FMEs also suggest that a depleted mantle or mantle-derived end-member was involved in petrogenesis (Faure and Mensing 2005). $^{87}Sr/^{86}Sr$ vs. SiO_2 (wt%), Sr (ppm) and $1/Sr \times 10^3$ (ppm $^{-1}$), and $^{143}Nd/^{144}Nd$ vs. Sm/Nd plots reveal the influence of fractional crystallization, rather than assimilation coupled with fractional crystallization, on the evolution of MHRs and FMEs (Fig. 10b–e).

Disequilibrium textures and the presence of FMEs also support the interaction and mixing/mingling of coeval mafic and felsic magma in the evolution of the stocks studied. Geochemically, mixing is evidenced by the remarkable overlap of data from MHR and FME samples in the $^{143}Nd/^{144}Nd$ vs. $^{87}Sr/^{86}Sr$ diagram (Fig. 10a). Linear correlations between some major elements and SiO_2 , as stated above (see Fig. 7), can also serve as evidence for magma mixing (McBirney 1980; Perugini and Poil 2004). The defined hyperbolic arrays on CaO vs. Rb, Nb/Ba vs. Th/Ta, MgO vs. Ni, Ce/Pb vs. La/Yb, Ti/Zr vs. Rb/Sr, and Al_2O_3/TiO_2 vs. TiO_2 plots, all of which are expected for the mixing between the two distinct

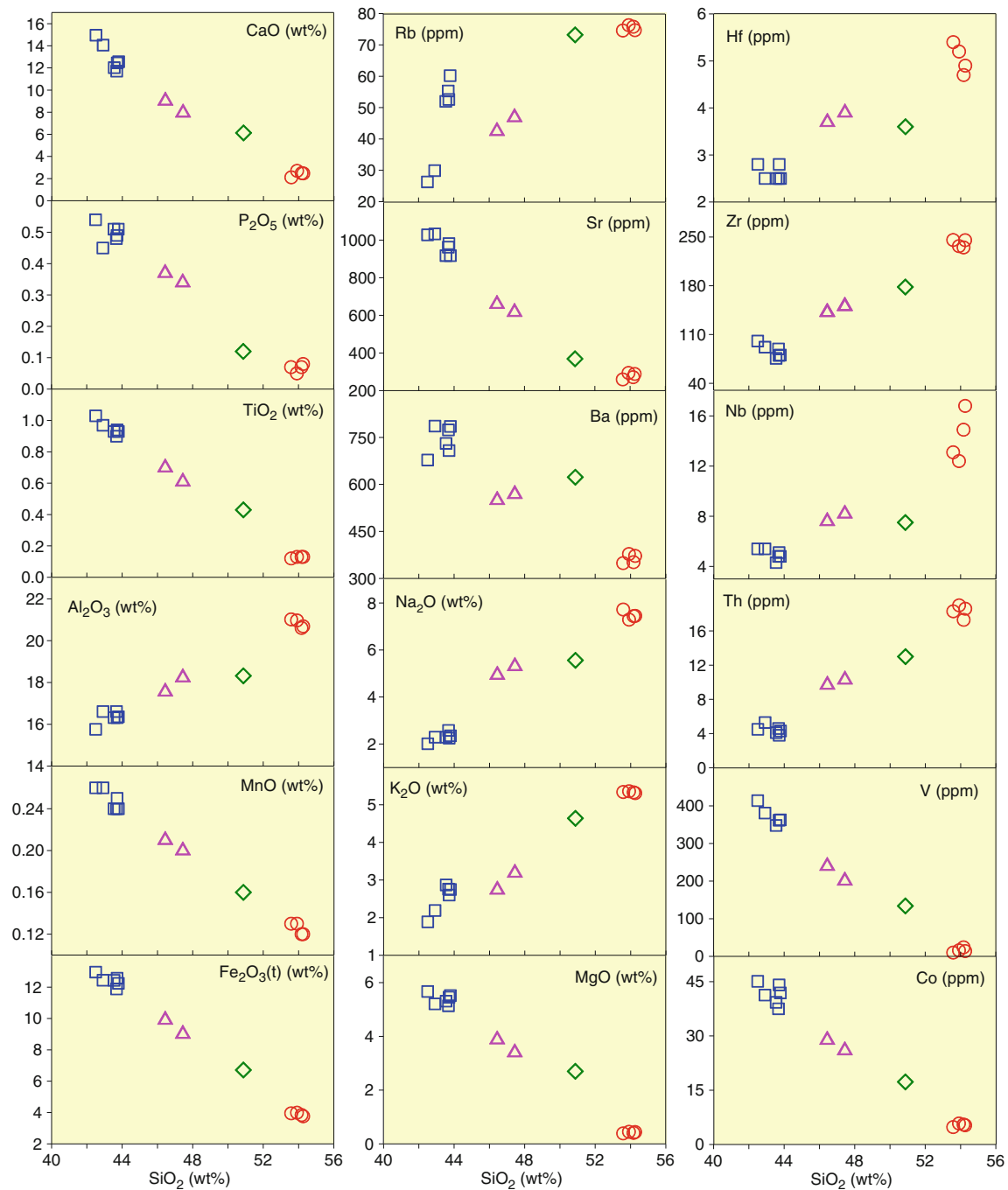


Fig. 7 SiO₂ (wt.%) vs. major oxide (wt.%), trace element (ppm) variation plots of the MHR, FME and contact samples from the Bafra (Samsun) area (symbols are as in Fig. 5a)

geochemical end-members, and are evidenced by the simple interaction between at least two magma types in genesis (Fig. 11a–f). In the host mafic magma, clinopyroxene, olivine, hornblende, and plagioclase crystallized prior to the injection of felsic magma. Petrographical data suggest that after the injection of felsic magma into mafic magma, bladed biotites were formed around the contact of mafic and felsic components to reach equilibrium conditions. The presence of reaction rims on the mafic minerals (i.e., clinopyroxene

and biotite), sieved textured plagioclase, and rounded and embayed mafic minerals were due to the intrusion of a small volume of felsic magma into the mafic magma chamber. Low-temperature felsic magma injection into mafic magma quenched the mafic magma and accumulated some bubbles at the felsic–mafic magma interface. Then, felsic magma foamed up, and plumes were found. In this entrainment, plumes were detached, forming rounded FMEs.

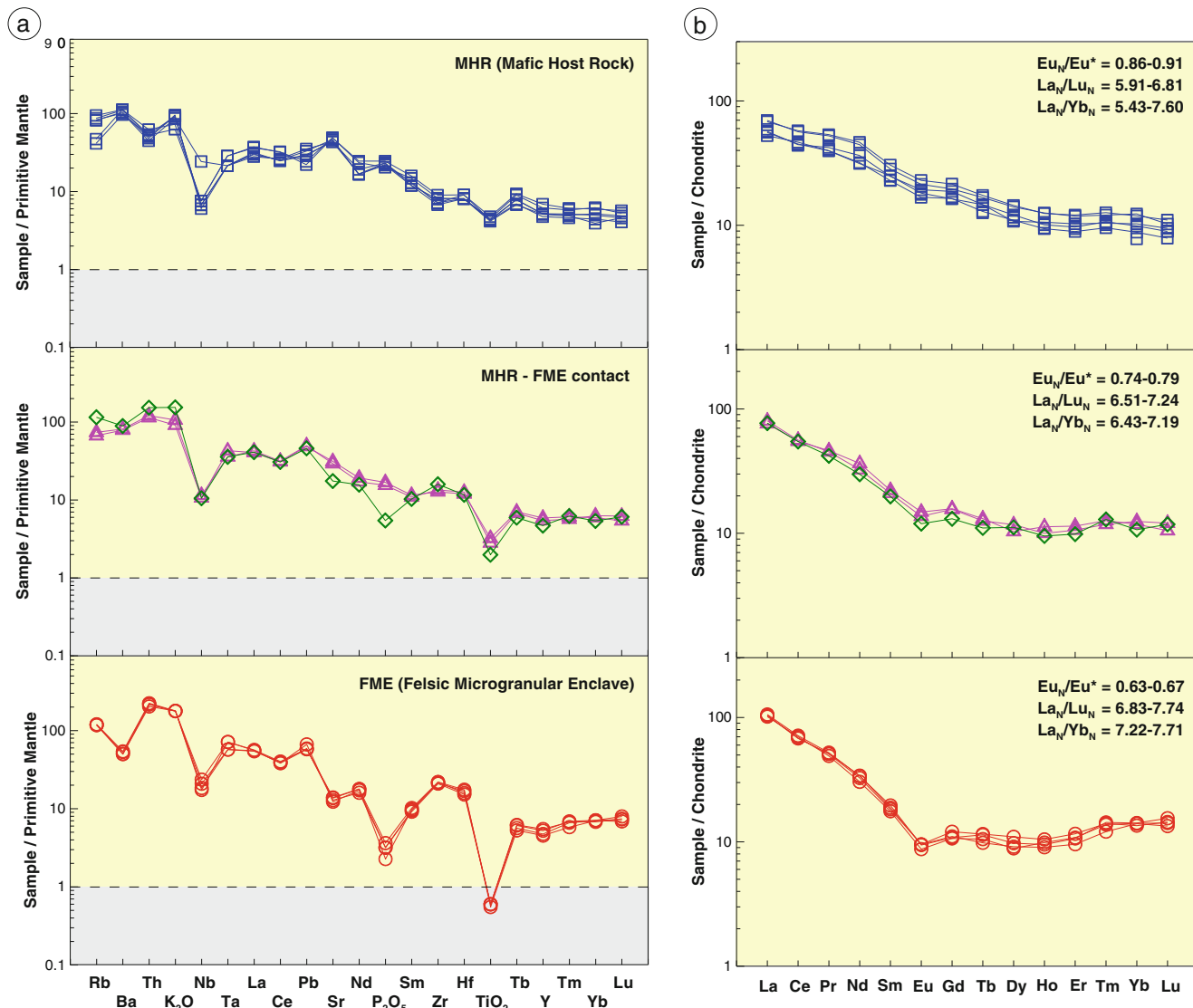


Fig. 8 **a** Primitive Mantle (Sun and McDonough 1989) normalized multi-element spider diagrams, and **b** chondrite (Taylor and McLennan 1985) normalized rare earth element patterns of the MHR, FME and contact samples from the Bafra (Samsun) area (symbols are as in Fig. 5a)

Characteristics and processes of magma mixing and mingling

The magma mingling/mixing event can be carefully detected through field and microscopic observations (Nardi and Lima 2000). A clear correlation also exists between the size and shape of FMEs and the degree of interaction between coeval magma types. According to field observations, smaller FMEs are wavy, flame-shaped rounded, or lobate, fine-grained, 5 cm to 20 cm in size, and 2 cm to 10 cm in diameter, indicating rapid undercooling or quenching. By contrast, large FMEs may be up to 10 cm in diameter, with more or less planar, elongated spherical, and ellipsoidal shapes and medium to fine grained (see Fig. 3a-f). FMEs come from the mixing/mingling of felsic and mafic magma (e.g., Vernon 1983; Barbarin and Didier 1992). On the other hand, Chappell and White (1992)

interpreted FMEs as remnants of partially melted igneous protolith. However, regarding the presence of anti-rapakivi and sieved plagioclase textures and acicular apatite crystals, FMEs in the study area are more plausibly a consequence of magma mixing/mingling. Moreover, these features may only suggest that magma mingling was the main factor in the generation of FMEs in the Bafra area as the difference between the temperature and density of mafic and felsic magma do not permit the complete mixing of the two magma types.

The contact between FMEs and MHRs are mainly sharp and irregular or diffuse with no signs of deformation (Fig. 4b), features that are commonly attributed to the undercooling and mingling of FMEs formed by a mixture of coeval mafic and felsic magma (e.g., Perugini et al. 2004). Key features of the rocks studied are the disequilibrium textures (Fig. 4d-i) of phenocrysts in MHRs and FMEs, which are considered

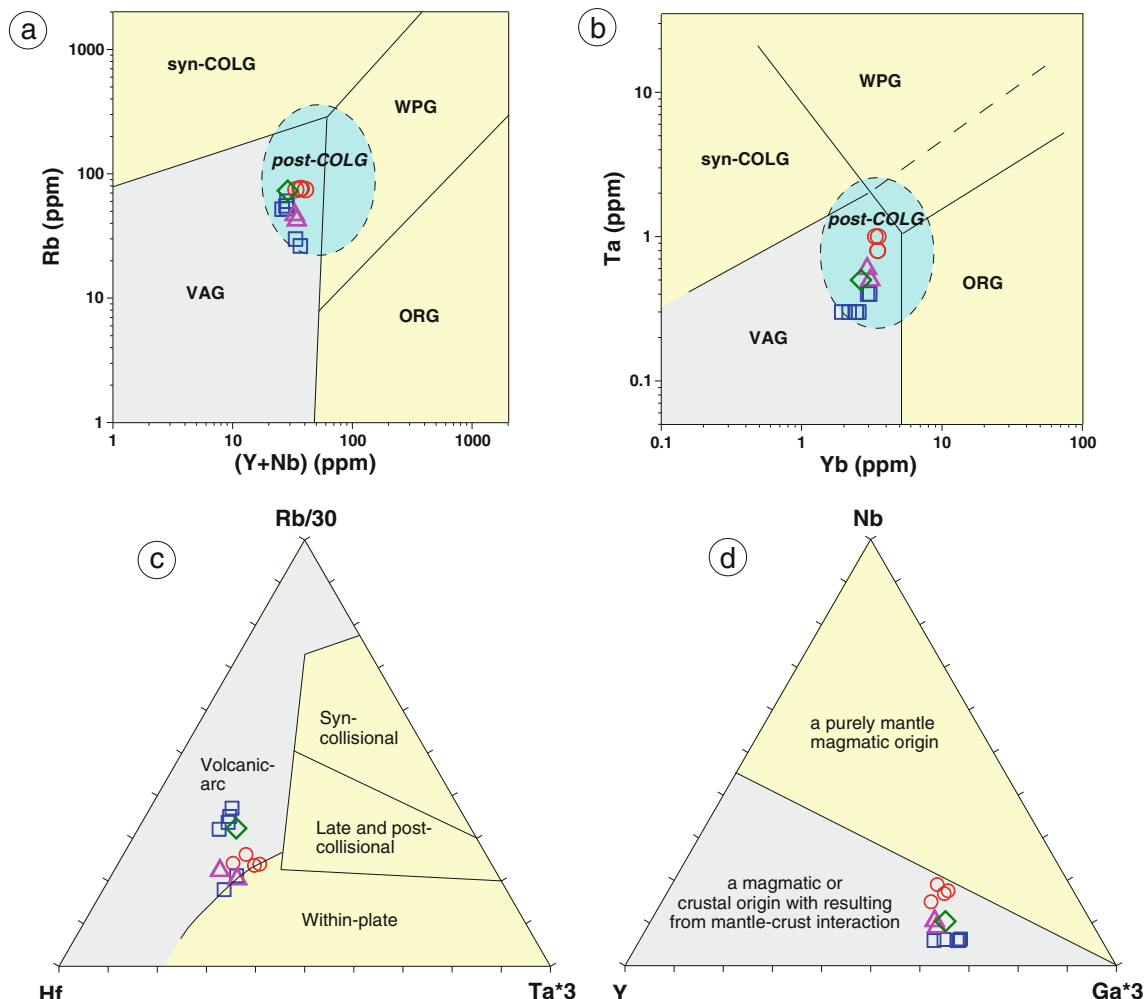


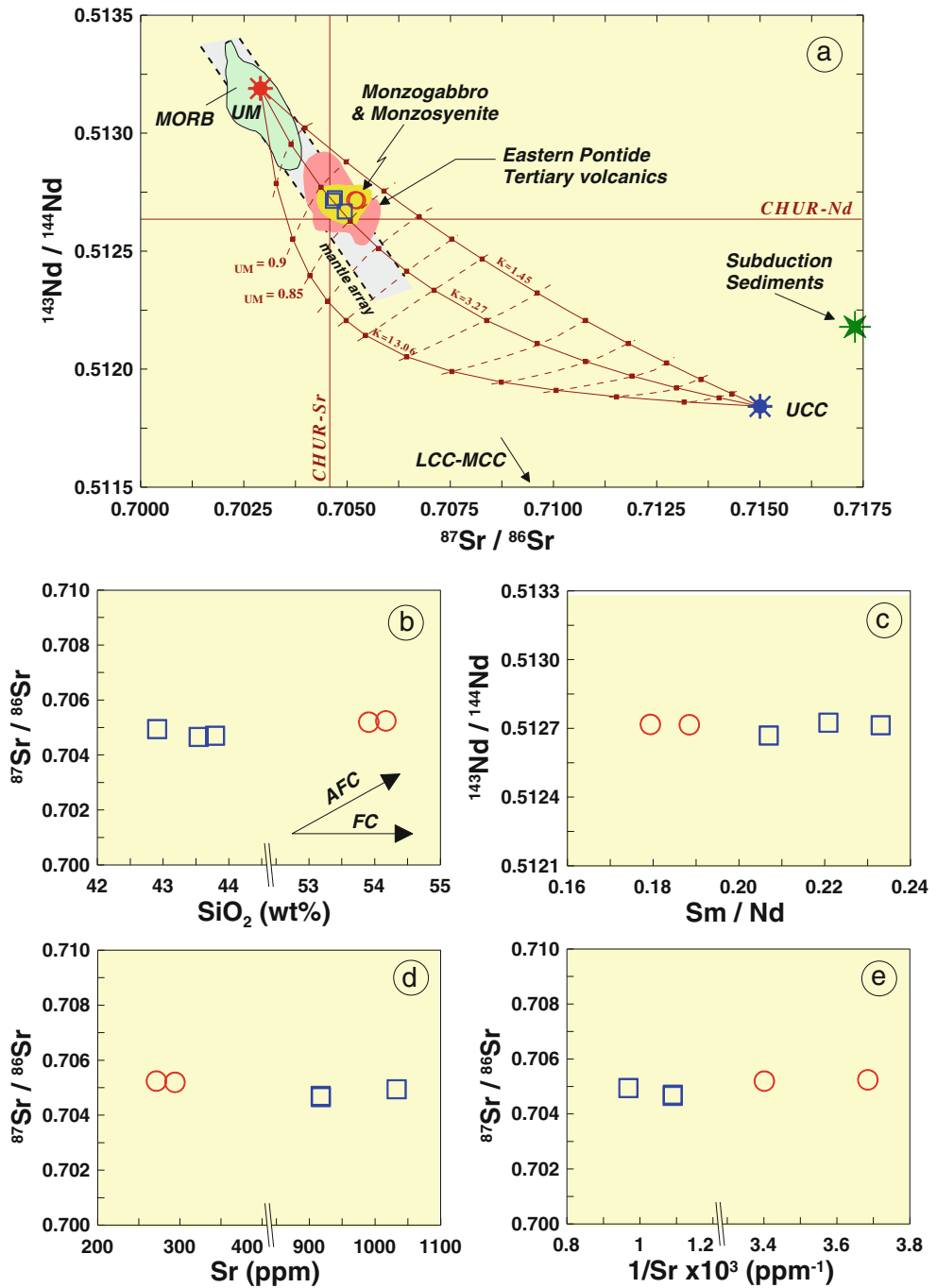
Fig. 9 **a** Rb (ppm) vs. (Y+Nb) (ppm) and **b** Ta (ppm) vs. Yb (ppm) trace element diagrams (after Pearce et al. 1984), **c** Rb/30-Hf-Ta*3 (after Harris et al. 1986) and **d** Nb-Y-Ga*3 (after Eby 1992) ternary diagrams for the MHR, FME and contact samples from the Bafrå

(Samsun) area; syn-COLG, syn-collisional granites; VAG, volcanic arc granite; WPG, within-plate granite; ORG, ocean ridge granite; post-COLG, post-collisional granite (symbols are as in Fig. 5a)

evidence of mixing/mingling. Disequilibrium textures, such as oscillatory and sector zoning in clinopyroxene megacryst, clinopyroxene rimmed by green hornblende, and relic clinopyroxene crystals, also occur in hornblende (Fig. 4d and h), embayed and breakdown clinopyroxene megacryst (Fig. 4d and i), and clinopyroxene mantled by bladed biotites (Fig. 4i) in MHRs, indicating the mixing/mingling of mafic and felsic magma. Plagioclase, which can resist high-temperature recrystallization (Cherniak and Watson 1992) and monitor changes in the physical-chemical environment during growth (Hibbard 1981; Janousek et al. 2000), provide important clues in the relation between FMEs and MHRs. Oscillatory zoning in plagioclase indicates variation in crystallization conditions (Holton et al. 1999). Debon (1991) and Hibbard (1991) noted that anti-rapakivi texture can be an evidence of magma hybridization and mingling. Sieve textured-patchy-rounded and corroded plagioclase (Fig. 4i) is evidence of mixing/mingling

(e.g., Dungan and Rhodes 1978; Tsuchiyama 1985). Spongy-textured plagioclase with a resorption zone (Fig. 4f, h and i) can be explained as a result of changes in magma chemistry caused by the mixing/mingling of mafic magma with a more acidic melt. As mafic magma invades the more acidic melt, strong undercooling can develop plagioclase crystals with patchy zoning (Hibbard 1995; Castro 2001). Patchy-zoned plagioclase phenocrysts are typical magma mixing textures (Vance 1965; Bussy 1990; Barbarin 1990) generated by plagioclase entering into a hotter, more basic magma, where partial dissolution of the Ab-rich component occurs in plagioclase. Alkali feldspar phenocrysts in FMEs do not necessarily imply late or subsolidus crystallization because experimental evidence shows that abundant liquid is available for crystal growth during alkali feldspar nucleation (Vernon and Paterson 2008). Some alkali feldspar phenocrysts contain euhedral and subhedral mineral inclusions of plagioclase, clinopyroxene,

Fig. 10 a $^{143}\text{Nd}/^{144}\text{Nd}$ vs. $^{87}\text{Sr}/^{86}\text{Sr}$ plot for the MHRs and FMEs. Also plotted for comparison are the samples from Tertiary Eastern Pontides volcanics (Kaygusuz et al. 2011; Temizel et al. 2012; Arslan et al. 2013; Aslan et al. (2013)). Compositions of MORB (Mid Ocean Ridge Basalt) and Mantle Array from Wilson (1989), Gill (1981) and McCulloch et al. (1994); UM (Upper Mantle) fields from (Klein 2004) and CHUR (Chondritic Uniform Reservoir)-Sr and -Nd reference lines after Zindler and Hart (1986). b $^{87}\text{Sr}/^{86}\text{Sr}$ vs. SiO_2 (wt.%), (c) $^{143}\text{Nd}/^{144}\text{Nd}$ vs. Sm/Nd , (d-e) $^{87}\text{Sr}/^{86}\text{Sr}$ vs. Sr (ppm) and $1/\text{Sr} \times 10^3$ (ppm $^{-1}$) diagrams showing possible fractional crystallization (FC) and assimilation-fractional crystallization (AFC) trends for the MHRs and FMEs from the Bafra (Samsun) area (symbols are as in Fig. 5a)



biotite, hornblende, sphene, Fe-Ti oxide and apatite (Fig. 4d), which suggests that alkali feldspar megacrysts grew while surrounded by melt, allowing inclusion minerals to periodically attach themselves to the faces of growing crystals (Moore and Sisson 2008). The identical composition of biotite and hornblende in FMEs and MHRs can be explained by crystallization under similar physical conditions (Barbarin 1986) or by diffusive reaction with late-stage melts. Large biotite crystals are found mainly along the periphery of FMEs (Fig. 4e), compared with plagioclase, which occurs everywhere in

FMEs. MHR biotite with identical size to large crystals in FMEs is commonly oriented tangentially to FME boundaries (Fig. 4e).

Even if mafic minerals are more elongated and acicular in MHRs, differences in size or shape may not necessarily imply variations in composition. Clinopyroxene is abundant in mafic host rocks. The dominance of hydrous minerals, such as hornblende and biotite, reflects H₂O-rich melt compositions for both FMEs and MHRs. Strong undercooling of mafic magma can also result in the growth of long prismatic apatite

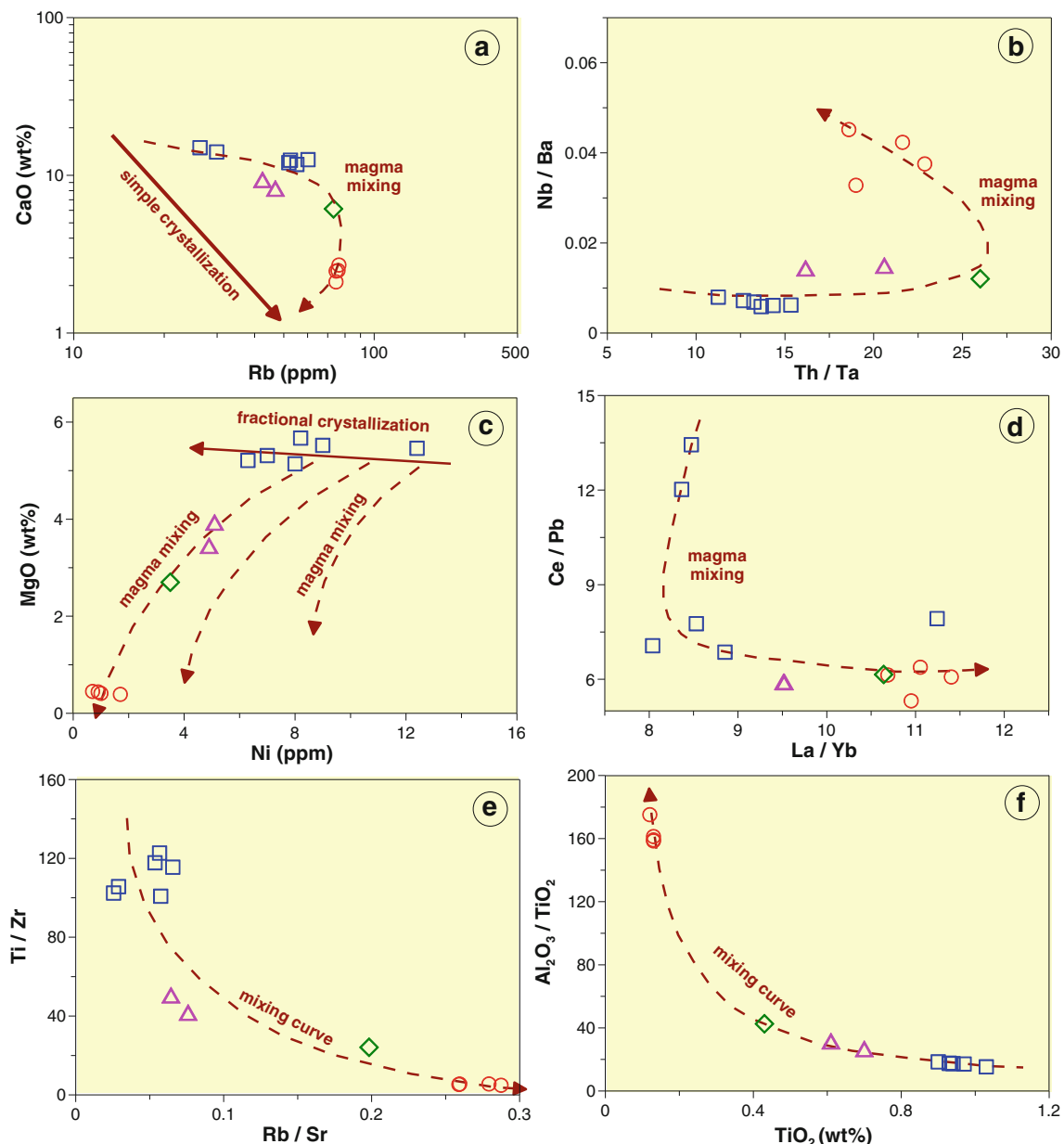


Fig. 11 **a** CaO vs. Rb, **b** Nb/Ba vs. Th/Ta, **c** MgO vs. Ni, **d** Ce/Pb vs. La/Yb, **e** Ti/Zr vs. Rb/Sr and **f** Al₂O₃/TiO₂ vs. TiO₂ plots of the MHR, FME and contact samples from the Bafra (Samsun) area (symbols are as in Fig. 5a)

(Fig. 4g). The presence of acicular apatites in MHRs (Fig. 4g) may be used as an indication of magma mingling (Vernon 1983; Janousek et al. 2000; Piccoli and Candela 2002).

If felsic enclaves in MHRs were cumulate rocks, then concentrations of elements such as Cr, Ni, Co, and Sr would be relatively high in the enclaves (Chappell 1996), which is not the case in the FMEs studied. Mineral grains in FMEs are also 5–10 times smaller than the same mineral phases in MHRs and do not show any cumulative texture, which suggests that fine-grained FMEs are not related to cumulate fractional crystallization (Kumar et al. 2004). A critical feature of the restite model is the existence of linear chemical variations (Chappell and

White 1992; Collins 1998), a feature not observed in the samples. Low abundance of refractory elements tends to accompany igneous microstructures, which also argues against a restitic origin for enclaves (Liankun and Kuirong 1991). Geochemical similarities between FMEs and MHRs may be explained if enclaves formed as cognate rocks (Fershtater and Borodina 1991), but this also does not appear to be the case in the stocks studied. Different petrographical and mineralogical data of MHRs and FMEs also indicate that these rocks do not have a restite or cognate origin, but were rather composed by two separated coeval magma types with various petrographical, mineralogical, and geochemical signatures.

Conclusions

It is envisaged for the first time from the petrographical and geochemical evidence that the coeval mafic and felsic magmas which resulted in Miocene aged phacolith-like gabbroic stocks and the felsic microgranular enclaves are derived from similar sources from the Bafra area at the western edge of the Eastern Pontides (NE Turkey).

The petrochemical contrasts between the FMEs and MHRs may in part be a consequence of extended interactions between coeval felsic and mafic magmas by mixing/mingling and diffusion. In addition, the enclave forming magma broke up into discrete globules, which likely entered the mafic magma chamber and formed enclaves in the mafic host either by convective motion in the host magma or by forceful injection. Felsic melts were at near liquidus conditions when injected into the mafic melts, and the gabbroic stocks (MHRs) reflect a hybrid product from mingling and partial (incomplete) mixing of these two melts. The Sr and Nd isotopic compositions of these rocks further suggest the involvement of lithospheric mantle-derived end-members in their petrogenesis.

Acknowledgments This study is a part of the project (Project No: 2010.112.5.3) supported by the Karadeniz Technical University Scientific Research Fund. The author would like to thank Mehmet Arslan for his thorough, critical, and constructive reviews and comments, which improved the manuscript. Special thanks are due to Emel Abdioğlu and Cem Yücel for their assistances during field work. The author also thanks to the chief editor J.G. Raith, the handling editor L.G. Gwalani and anonymous reviewers for their critical and constructive comments.

References

- Arslan M, Temizel İ, Abdioğlu E, Kolaylı H, Yücel C, Boztuğ D, Şen C (2013) ^{40}Ar - ^{39}Ar dating, whole-rock and Sr-Nd-Pb isotope geochemistry of post-collisional Eocene volcanics in the southern part of the Eastern Pontides (NE Turkey): implications for magma evolution in extension-induced origin. Contrib Mineral Petrol 166:113–142
- Arslan M, Aslan Z (2006) Mineralogy, petrography and whole-rock geochemistry of the Tertiary granitic intrusions in the Eastern Pontides, Turkey. J Asian Earth Sci 27:177–193
- Aslan Z, Arslan M, Temizel İ, Kaygusuz A (2013) K-Ar age, whole-rock, and Sr-Nd isotope geochemistry of calc-alkaline volcanic rocks around the Gümüşhane area (Northeast Turkey): implications for post-collisional volcanism during Tertiary time in the Eastern Pontides. Mineral Petrol. doi:[10.1007/s00710-013-0294-2](https://doi.org/10.1007/s00710-013-0294-2)
- Bacon CR (1986) Magmatic inclusions in silicic and intermediate volcanic rocks. J Geophys Res 91:6091–6112
- Bacon CR, Metz J (1984) Magmatic inclusions in rhyolites, contaminated basalts, and compositional zonation beneath the Coso volcanic field, California. Contrib Mineral Petrol 85:46–365
- Barbarin B (1986) Comparison of mineralogy of mafic magmatic enclaves and host granitoids, central Sierra Nevada, California. Abstracts of the Geological Society of America Annual Meeting 18:83
- Barbarin B (1990) Plagioclase xenocrysts and mafic magmatic enclaves in some granitoids of the Sierra Nevada Batholith, California. J Geophys Res 95:17747–17756
- Barbarin B, Didier J (1992) Genesis and evolution of mafic microgranular enclaves through various types of interaction between co-existing felsic and mafic magmas. Trans R Soc Edinb Earth Sci 83:145–153
- Best MG (2006) Igneous and metamorphic petrology, 2nd edn. Blackwell, USA, 729
- Blake S, Fink JH (2000) On the deformation and freezing of enclaves during magma mixing. J Volcanol Geoth Res 95:1–8
- Borg LE, Nyquist LE, Wiesmann H, Shih CY (1997) Constraints on Martian differentiation processes from Rb-Sr and Sm-Nd isotopic analyses of the basaltic shergottite QUE94201. Geochim Cosmochim Acta 61:4915–4931
- Bozkurt E, Mittwede SK (2001) Introduction to the geology of Turkey—a synthesis. Int Geol Rev 43:578–594
- Boztuğ D, Kuşcu İ, Erçin Aİ, Avcı N (2003) Mineral deposits associated with the pre-, syn- and post-collisional granitoids of the Neo-Tethyan convergence system between the Eurasian and Anatolian plates in NE and Central Turkey. In: Eliopoulos D et al (eds) Mineral exploration and sustainable development. Millpress, Rotterdam, pp 1141–1144
- Boztuğ D, Jonckheere R, Wagner GA, Yeğençil Z (2004) Slow Senonian and fast Paleocene-Early Eocene uplift of the granitoids in the Central Eastern Pontides, Turkey: apatite fission-track results. Tectonophysics 382:213–228
- Boztuğ D, Jonckheere RC, Arslan M, Şen C, Karslı O, Erçin Aİ (2005) Eocene slab break-off revealed by the E-W distribution of the multi-sourced granitoids and tectonic denudation in the eastern Pontides, Turkey. Geophys Res Abstr 7:02129
- Boztuğ D, Erçin Aİ, Kuruçelik MK, Göç D, Kömür İ, İskenderoğlu A (2006) Geochemical characteristics of the composite Kaçkar batholith generated in a Neo-Tethyan convergence system, Eastern Pontides, Turkey. J Asian Earth Sci 27:286–302
- Boztuğ D, Jonckheere RC, Wagner GA, Erçin Aİ, Yeğençil Z (2007) Titanite and zircon fission-track dating resolves successive igneous episodes in the formation of the composite Kaçkar batholith in the Turkish Eastern Pontides. Int J Earth Sci 96:875–886
- Boztuğ D, Harlavan Y (2008) K-Ar ages of granitoids unravel the stages of Neo-Tethyan convergence in the eastern Pontides and central Anatolia, Turkey. Int J Earth Sci 97:585–599
- Bussy F (1990) Petrogenèse des enclaves microgrenues associées aux granitoides calco-alcalins: exemples des massifs varisques du Mont-Blanc (Alpes occidentales) et Miocene du Monte Capanne (Iled'Elbe, Italie). Ph.D. Thesis, Memoire de Géologie, Lausanne
- Castro A (2001) Plagioclase morphologies in assimilation experiments: implications for disequilibrium melting in the generation of granodiorite rocks. Mineral Petrol 71:31–49
- Chappell BW (1996) Magma mixing and the production of compositional variation within granite suites: evidence from the granites of southeastern Australia. J Petrol 37:449–470
- Chappell BW, White AJR (1974) Two contrasting granite types. Pac Geol 8:173–174
- Chappell BW, White AJR (1992) I- and S-type granites in the Lachlan Fold Belt. Trans R Soc Edinb Earth Sci 83:1–26
- Cherniak DJ, Watson EB (1992) A study of strontium diffusion in K-feldspar, Na-K feldspar and anorthite using Rutherford Backscattering Spectroscopy. Earth Planet Sci Lett 113:411–425
- Collins WJ (1998) Evaluation of petrogenetic models for Lachlan Fold Belt granitoids: implications for crustal architecture and tectonic models. Aust J Earth Sci 45:483–500
- Debon F (1991) Comparative major element chemistry in various “microgranular enclave-plutonic host” pairs. In: Didier J, Barbarin B (eds) Enclaves and granite petrology. Elsevier, Amsterdam, pp 293–312

- De Rosa R, Donato P, Ventura G (2002) Fractal analysis of mingled/mixed magmas: an example from the Upper Polara eruption (Sala Island, southern Tyrrhenian Sea, Italy). *Lithos* 65:299–311
- Dokuz A, Tanyolu E, Genç S (2006) A mantle- and a lower crust-derived bimodal suite in the Yusufeli (Artvin) area, NE Turkey: trace element and REE evidence for subduction-related rift origin of Early Jurassic Demirkent intrusive complex. *Intern Earth Sci* 95:370–394
- Dungan MA, Rhodes JM (1978) Residual glasses and melt inclusions in basalts from DSDP Leg 45 and 46: evidence for magma mixing. *Contrib Mineral Petrol* 67:417–431
- Eby GN (1992) Chemical subdivision of the A-type granitoids: petrogenetic and tectonic implications. *Geology* 20:641–644
- Eichelberger JC (1978) Andesitic volcanism and crustal evolution. *Nature* 275:21–22
- Eichelberger JC, Chertkoff DG, Dreher ST, Nye CJ (2000) Magmas in collision: rethinking chemical zonation in silicic magmas. *Geology* 28:603–606
- Faure G, Mensing TM (2005) Isotopes: Principles and applications, 3rd edn. Wiley, USA, 897p
- Fershtater GB, Borodina NS (1991) Enclave in the Hercynian granitoids of the Urals Mountains, U.S.S.R. In: Didier J, Barbarin B (eds) *Enclaves and granite petrology*. Elsevier, Amsterdam, pp 83–94
- Floyd RA, Göncüoğlu MC, Winchester JA, Yalnız MK (2000) Geochemical character and tectonic environment of Neotethyan ophiolitic fragments and metabasites in the Central Anatolian Crystalline Complex, Turkey. In: Bozkurt E, Winchester JA (Eds.), *Tectonics and Magmatism in Turkey and the surrounding area*. Geol Soc London Spec Publ 173:182–202
- Frost TP, Mahood GA (1987) Style of mafic-felsic magma interaction: the lamarc Granodiorite, Sierra Nevada, California. *Geo Soc Am Bull* 99:272–291
- Gedik A, Ercan T, Korkmaz S (1984) Orta Karadeniz (Samsun-Sinop) havzasının jeolojisi ve volkanik kayaçlarının petrolojisi. MTA Enst Derg 99–100:34–50
- Gedik A, Korkmaz S (1984) Sinop havzasının jeolojisi ve petrol olanakları, MTA Rapor No: 7575
- Gill JB (1981) Orogenic andesites and plate tectonics. Springer, Berlin, 390p
- Grove TL, Donnelly-Nolan JM (1986) The evolution of young silicic lavas at Medicine Lake Volcano, California: implications for the origin of compositional gaps in calc-alkaline series lavas. *Contrib Mineral Petrol* 92:281–302
- Güven İH (1993) 1:25000-Scale geological and metallogenical map of the eastern Black Sea Region. Mineral Research and Exploration Institute of Turkey. (MTA) Publications, Ankara, Turkey, p 98
- Harris NBW, Pearce JA, Tindle AG (1986) Geochemical characteristics of collision-zone magmatism. In: Coward M P, Ries A C (eds.), *Collision Tectonics*. Geol Soc London Spec Publ 19:67–81
- Heiken G, Eichelberger JC (1980) Eruptions at Chaos Crags, Lassen Volcanic National Park, California. *J Volcanol Geoth Res* 7:443–481
- Hibbard MJ (1981) The magma mixing origin of mantled feldspars. *Contrib Mineral Petrol* 76:158–170
- Hibbard MJ (1991) Textural anatomy of twelve magma-mixed granitoid systems. In: Didier J, Barbarin B (eds) *Enclaves and granite petrology*. Elsevier, Amsterdam, pp 431–444
- Hibbard MJ (1995) Petrography to petrogenesis. Prentice Hall, New Jersey
- Holton T, Jamtveit B, Meakin P (1999) Noise and oscillatory zoning of minerals. *Geochim Cosmochim Acta* 64:1893–1904
- Irvine TN, Baragar WRA (1971) A guide to the chemical classification of common volcanic rocks. *Can J Earth Sci* 8:523–548
- Jacobsen SB, Wasserburg GJ (1980) Sm-Nd isotopic evolution of chondrites. *Earth Planet Sci Lett* 50:139–155
- Janousek V, Bowes DR, Braithwaite CJR, Rogers G (2000) Microstructural and mineralogical evidence for limited involvement of magma mixing in the petrogenesis of a Hercynian high-K calc-alkaline intrusion: the Kozarovice granodiorite, Central Bohemian Pluton, Czech Republic. *Trans R Soc Edinb Earth Sci* 91:15–26
- Kaygusuz A, Aslan Z, Siebel W, Şen C (2011) Geochemical and Sr-Nd Isotopic Characteristics of Post-Collisional Calc-Alkaline Volcanics in the Eastern Pontides (NE Turkey). *Turkish J Earth Sci* 20:137–159
- Klein EM (2004) Geochemistry of the igneous oceanic crust, In: *Treatise on Geochemistry*. Holland HD, Turekian KK (Eds.), Elsevier, Amsterdam 3:433–463
- Kumar S, Rino V, Pal AB (2004) Field evidence of magma mixing from microgranular enclaves hosted in Palaeoproterozoic Malanjkhand granitoids, central India. *Gondwana Res* 7:539–548
- Liankun S, Kuirong Y (1991) A two-stage crust-mantle interaction model for mafic microgranular enclaves in the Donging granodiorite Pluton, Guangxi, China. In: Didier J, Barbarin B (eds) *Enclaves and granite petrology*. Elsevier, Amsterdam, pp 95–112
- Liégeois JP, Black R (1987) Alkaline magmatism subsequent to collision in the Pan-african belt of the Adrar des Iforas (Mali). In: Fitton JG, Upton BJG (Eds.), *Alkaline igneous rocks*. Geol Soc London Spec Publ 30:381–401
- Liew TC, Hofmann AW (1988) Precambrian crustal components, plutonic associations, plate environment of the Hercynian Fold Belt of central Europe: indications from a Nd and Sr isotopic study. *Contrib Mineral Petrol* 98:129–138
- Macdonald R, Belkin HE, Fitton JG, Rogers NW, Nejbert K, Tindle AG, Marshal AS (2008) The role of fractional crystallization, magma mixing, crystal mush remobilization and volatile-melt interactions in the genesis of young basalt-peralkaline rhyolite suite, the Great Olkaria Volcanic Complex, Kenya Rift Valley. *J Petrol* 49:1515–1547
- McBirney AR (1980) Mixing and unmixing of magmas. *J Volcanol Geoth Res* 7(3–4):357–371
- Mcculloch MT, Gamble JA (1991) Geochemical and geodynamical constraints on subduction zone magmatism. *Earth Planet Sci Lett* 102:358–374
- McCulloch MT, Kyser TK, Woodhead JD, Kinsley L (1994) Pb-Sr-Nd-O Isotopic Constraints on the Origin of Rhyolites from the Taupo Volcanic Zone of New Zealand: evidence for assimilation followed by fractionation of basalt. *Contrib Mineral Petrol* 115:303–312
- Middlemost EAK (1994) Naming materials in the magma/igneous rock system. *Earth Sci Rev* 37:215–224
- Miyashiro A (1978) Nature of alkalic volcanic rock series. *Contrib Mineral Petrol* 66:91–104
- Moore JG, Sisson TW (2008) Igneous phenocrystic origin of K-feldspar megacrysts in granitic rocks from the Sierra Nevada batholith. *Geosphere* 4:387–400
- Nardi LVS, Lima EF (2000) Hybridisation of microgranular enclaves in the Lavras Granite Complex, southern Brazil. *J South Am Earth Sci* 13:67–78
- Nixon GT, Pearce TH (1987) Laser-interferometry study of oscillatory zoning in plagioclase: The record of magma mixing and phenocryst recycling in calc-alkaline magma chambers, Iztaccihuatl volcano, Mexico. *Am Miner* 72:1144–1162
- Okay Aİ, Şahintürk Ö (1997) Geology of the eastern Pontides, in: Robinson AG (Ed.), *Regional and Petroleum Geology of the Black Sea and Surrounding Region*. AAPG Memoir 68:291–311
- Okay Aİ, Tansel İ, Tüysüz O (2001) Obduction, subduction and collision as reflected in the Upper Cretaceous–Lower Eocene sedimentary record of western Turkey. *Geol Mag* 138:117–142
- Okay Aİ, Tüysüz O (1999) Tethyan sutures of northern Turkey. *Geol Soc London Spec Publ* 156:475–515
- Pearce JA (1982) Trace element characteristics of lavas from destructive plate boundaries. In: Thorp RS (ed) *Andesites: Orogenic andesites and related rocks*. Wiley, New York, pp 525–548, 724 p

- Pearce JA (1996) A user's guide to basalt discrimination diagrams. In: Wyman DA (ed.) Trace Element Geochemistry of Volcanic Rocks: Applications for Massive Sulphide Exploration. Geological Association of Canada, Short Course Notes 12:79–113
- Pearce JA, Harris NBW, Tindle AG (1984) Trace element discrimination diagrams for the tectonic interpretation of granitic rocks. *J Petrol* 25:956–983
- Pearce JA, Bender JF, De Long SE, Kidd WSF, Low PJ, Güner Y, Saroğlu F, Yilmaz Y, Moorbat S, Mitchell JJ (1990) Genesis of collision volcanism in eastern Anatolia Turkey. *J Volcanol Geoth Res* 44:189–229
- Pearce JA, Peate DW (1995) Tectonic implications of the composition of volcanic arc magmas. *Ann Rev Earth Planet Sci* 23:251–285
- Perugini D, Poil G (2004) Analysis and numerical simulation of chaotic advection and chemical diffusion during magma mixing: petrological implications. *Lithos* 78(1–2):43–66
- Perugini D, Ventura G, Petrelli M, Poli G (2004) Kinematic significance of morphological structures generated by mixing of magmas: a case study from Salina Island (southern Italy). *Earth Planet Sci Lett* 222:1051–1066
- Piccoli PM, Candela PA (2002) Apatite in igneous system. *Rev Mineral Geochem* 48:255–292
- Poli G, Tommasini S, Halliday AN (1996) Trace elements and isotopic exchange during acid-basic magma interaction processes. *Trans R Soc Edinb Earth Sci* 87:225–232
- Robinson DM, Miller CF (1999) Record of magma chamber processes preserved in accessory mineral assemblages. *Am Miner* 84:1346–1353
- Sakuyama M (1981) Petrological study of the Myoko and Kurochime volcanoes, Japan: crystallization sequences and evidence for magma mixing. *J Petrol* 22:553–583
- Singer BS, Dingan MA, Layne GD (1995) Textures and Sr, Ba, Mg, Fe, K, and Ti compositional profiles in volcanic plagioclase: clues to the dynamics of calc-alkaline magma chambers. *Am Miner* 80:776–798
- Sparks RSJ, Marshall LA (1986) Thermal and mechanical constraints on mixing between mafic and silicic magmas. *J Volcanol Geotherm Res* 29:99–124
- Sparks RSJ, Sigurdsson SH, Wilson L (1977) Magma mixing: a mechanism for triggering acid explosive eruptions. *Nature* 267:315–318
- Sun SS, McDonough WF (1989) Chemical and isotopic systematics of oceanic basalts: implications for mantle composition and processes. In: Saunders AD, Norry MJ (Eds.), *Magmatism in the Ocean Basins*. Geol Soc London Spec Publ 42:313–345
- Şengör AMC, Yilmaz Y (1981) Tethyan evolution of Turkey: a plate tectonic approach. *Tectonophysics* 75:181–241
- Taylor SR, McLennan SM (1985) The continental crust: Its composition and evolution. Blackwell, Scientific Publication, Oxford, 312
- Temizel İ, Arslan M, Ruffet G, Peucat JJ (2012) Petrochemistry, geochronology and Sr-Nd isotopic systematics of the Tertiary collisional and post-collisional volcanic rocks from the Ulubey (Ordu) area, eastern Pontide, NE Turkey: implications for extension-related origin and mantle source characteristics. *Lithos* 128:126–147
- Thirlwall MF, Smith TE, Graham AM, Theodorou N, Hollings P, Davidson JP, Arculus RJ (1994) High field strength element anomalies in arc lavas; source or process? *J Petrol* 35:819–838
- Thomas N, Tait SR (1997) The dimensions of magmatic inclusions as a constraint on the physical mechanism of mixing. *J Volcanol Geoth Res* 75:167–178
- Tsuchiyama A (1985) Dissolution kinetics of plagioclase in the melt of the system diopside-albite-anorthite, and origin of dusty plagioclase in andesites. *Contrib Mineral Petrol* 89:1–16
- Topuz G, Altherr R, Schwarz WH, Siebel W, Satır M, Dokuz A (2005) Post-collisional plutonism with adakite-like signatures: the Eocene Saraycık granodiorite (Eastern Pontides, Turkey). *Contrib Mineral Petrol* 150:441–455
- Topuz G, Okay AI, Altherr R, Schwarz WH, Siebel W, Zack T, Satır M, Şen C (2011) Early Eocene post-collisional adakite-like magmatism in the Ağvanis Massif (Eastern Pontides, Turkey) and implications for the evolution of the Eocene magmatism. *Lithos* 125:131–150
- Vance JA (1965) Zoning in igneous plagioclase: patchy zoning. *J Geol* 73:636–651
- Vernon RH (1983) Restite, xenoliths and microgranitoid enclaves in granites. *J Proc Roy Soc New S Wales* 116:77–103
- Vernon RH, Paterson SR (2008) How late are K-feldspar megacrysts in granites? *Lithos* 104:327–336
- Weinberg RF, Sial AN, Pessoa RR (2001) Magma flow within the traverse pluton, northeastern Brazil: compositional and thermal convection. *Geol Soc Am Bull* 113:508–520
- Weis D, Kieffer B, Maerschalk C, Barling J, de Jong J, Willians GA, Hanano D, Pretorius W, Scoates JS, Goolaerts A, Friedman RM, Mahoney JB (2006) High-precision isotopic characterization of USGS reference materials by TIMS and MC-ICP-MS. *Geochem Geophys Geosyst* 7:1–30
- Williams Q, Tobisch OT (1994) Microgranitic enclave shapes and magmatic strain histories: constraints from drop deformation theory. *J Geophys Res* 99:24359–24368
- Wilson M (1989) Igneous petrogenesis. Oxford University Press, Oxford, 466pp
- Yağcıoğlu UC, Abdioğlu E, Arslan M, Schroeder PA (2012) Mineralogy and chemistry of the zeolites and associated minerals in the Tekkeköy (Samsun) volcanics, N Turkey: preliminary results. Proceedings of 15th National Clay Symposium p. 371–372
- Yilmaz Y (1972) Petrology and structure of the Gümüşhane granite and the surrounding rocks. NE Anatolia, PhD Thesis University College London, England. 248 pp
- Yilmaz S, Boztug D (1996) Space and time relations of three plutonic phases in the Eastern Pontides, Turkey. *Int Geol Rev* 38:935–956
- Yilmaz Y, Tüysüz O, Yiğitbaş E, Genç ŞC, Şengör AMC (1997) Geology and tectonics of the Pontides. In: Robinson AG (Ed.), *Regional and Petroleum Geology of the Black Sea and Surrounding Region*. AAPG Memoir 68:183–226
- Yilmaz-Şahin S, Güngör Y, Boztug D (2004) Comparative petrogenetic investigation of Composite Kaçkar Batholith granitoids in Eastern Pontide magmatic arc-Northern Turkey. *Earth Planets Space* 56:429–446
- Yoldaş R, Balkıray K, Granit S, Korkmaz S, Didik S, Kalkan İ, Ağrıdağ DS, Besbelli B (1985) Samsun ve dolayının (Kızılırmak-Yesilirmak arasındaki Bölgenin) jeolojisi ve petrol olanaklarına ilişkin rapor, MTARapor No: 8130
- Zindler A, Hart SR (1986) Chemical geodynamics. *Ann Rev Earth Planet Sci* 14:493–571